Can a flower color ancestral polymorphism transcend speciation?

Mercedes Sánchez-Cabrera[1], Eduardo Narbona[2], Montserrat Arista[1], Pedro L. Ortiz[1], Francisco J. Jiménez-López[3], Amelia Fuller[4], Benjamin Carter[5], and Justen B. Whittall[6*]

[1]Department of Plant Biology and Ecology, Universidad de Sevilla, Seville, Spain 41012

[2]Department of Molecular Biology and Biochemical Engineering, Pablo de Olavide University, Seville, Spain 41013

[3]Departamento de Biología, Geología, Física y Química Inorgánica, Universidad Rey Juan Carlos, Móstoles, Spain

[4]Department of Chemistry and Biochemistry, Santa Clara University, Santa Clara, CA 95053

[5]Department of Biological Sciences, San Jose State University, Santa Jose, CA 95182

[6]Department of Biology, Santa Clara University, Santa Clara, CA 95053

[*]**Corresponding Author:** jwhittall@scu.edu

Abstract

Polymorphisms are common in nature, but they are rarely shared among related species. They could originate through convergence, ancestral polymorphism, or introgression. Although shared neutral genomic variation is commonplace, very few examples of shared functional traits exist. The blue-orange petal colors polymorphisms in two closely related species, *Lysimachia monelli* and *L. arvensis* were investigated with UV-vis reflectance spectra, flavonoid biochemistry, and transcriptome comparisons followed by climate niche analysis. The similarities in reflectance spectra, biochemistry, and transcriptomes suggest a single shift from blue-to-orange shared by both lineages is possible. Transcriptome comparisons reveal two orange-specific genes are directly involved in both blue-orange color polymorphisms: *DFR-2* specificity redirects flux from the malvidin to the pelargonidin while *BZ1-2* stabilizes it with glucose, producing the orange pelargonidin 3-glucoside. The climate niches for each color morph are the same between the two species for three temperature characteristics but differ for four precipitation variables. We suggest that this persistent flower color polymorphism may represent an ancestrally polymorphic trait that has transcended speciation with some unique ecological effects.

Keywords: ancestral polymorphism, anthocyanin, flavonoid, *Lysimachia arvensis*, *Lysimachia monelli*, petal transcriptome

Introduction

Since the Modern Synthesis, we have assumed that most phenotypic variation emerges within populations and is subsequently acted upon by evolutionary forces within species (Dobzhansky, 1937; Grant, 1981). Herein, we describe an ancestral flower color polymorphism that may have transcended the species boundary providing a concrete example of unsorted ancient phenotypic variation in two species with contrasting ecological effects. This study addresses how shared traits evolve across lineages, a central topic in understanding the evolution of biological diversity.

Polymorphisms, or variation among individuals of the same species, provide rare windows into the process of adaptation and speciation (Allison, 1961; Igić et al., 2008; Martin et al., 2013; Comeault et al., 2015). Polymorphisms among individuals in a population or among populations of a single species, are omnipresent across the tree of life (McKinnon & Pierotti, 2010; McLean & Stuart-Fox, 2014) and can be maintained by a diversity of forces including negative frequency-dependent selection (Madsen et al., 2022), heterozygote advantage (Sirugo et al., 2014), genetic drift (Wright, 1943, but see Schemske & Bierzychudek, 2007), gene flow (Martin et al., 2013) and spatially or temporally variable selection (Svensson, 2017). Some polymorphisms are phylogenetically dispersed (e.g. bird plumage color or flower color; Hugall & Stuart-Fox, 2012), while in others reoccur in very closely related species (e.g. heterostyly in *Primula*, shell chirality in *Amphidromus*, cryptic body color polymorphisms in *Timema* walking sticks, and wing patterning in *Heliconius* butterflies; reviewed in Jamie & Meier, 2020). The molecular underpinnings, persistence mechanics and evolutionary forces acting on these rare cases of shared variation are largely unexplored.

Some studies have proposed that polymorphisms promote the utilization of a wide range of environmental resources and can act as a precursor to speciation which then become fixed after divergence (Corl et al., 2010; Hugall & Stuart-Fox, 2012; McLean & Stuart-Fox, 2014). However, polymorphisms that persist across species (Jamie & Meier, 2020) represent evolutionary enigmas. How can polymorphisms transcend species boundaries? Convergent evolution (Gould, 1989; Conway, 2005) including developmental convergence (i.e. independent changes in gene expression), introgression (Mallet, 2005; Nolte et al., 2009), and the maintenance of an ancestral polymorphism (Igić & Kohn,

2001; Igić et al., 2008) are three plausible evolutionary avenues leading to shared polymorphisms among closely related species.

Color polymorphisms are widespread in nature but only a few cases of trans-specific color polymorphisms have been reported, and mostly restricted to animals (reviewed in McKinnon & Pierotti, 2010; Martin et al., 2013; McLean & Stuart-Fox, 2014; McRobie et al., 2019). Few examples have been investigated in plants. The closest situation for flower color is the repeated transitions from blue to red flowers (Wessinger & Rausher, 2013) associated with shifts from bee- to hummingbird-pollination (Thompson & Wilson, 2008; Muchhala et al., 2014; Wessinger et al., 2019) in a diversity of angiosperm lineages. However, in this case actual blue-red flower color polymorphisms (variation within populations) are very rare since either (1) multiple mutations are required to accomplish this shift and/or (2) the color is associated with a pollinator shift leading to reproductive isolation between the color types thereby fixing the color differences in newly formed species (but see Stankowski and Streisfeld 2015).

Unlike the blue to red flower color transitions leading to speciation, the blue-orange flower color polymorphism in the closely related species *Lysimachia arvensis* and *L. monelli* (*La* and *Lm* herein, Figure 1A) does not confer a pollinator shift (Jiménez-López et al., 2019; Sánchez-Cabrera, 2023). Instead, in *La* the color polymorphism is driven by abiotic non-pollinator agents of selection such as drought and sunlight intensity (Arista et al., 2013, Ortiz et al., 2015) and temperature (Jiménez-López et al., 2023; B. Carter et al., unpublished data) where blue flowered individuals are fitter than orange ones in drier, sunnier and hotter environments. *La*, is an annual native to the Mediterranean Basin and central and northern Europe. A recent autopolyploid origin has been suggested for *La* for three reasons: (1) due to the lack of ITS polymorphisms (Jiménez-López et al., 2022), (2) the presence of four identical copies of one set of chromosomes (Monein et al., 2003), (3) and the phylogenetic configuration of the group (Jiménez-López et al., 2022). Color morph frequencies range from 0% to 100% with a steep cline in central-southern Mediterranean region where mixed populations are common (e.g., Portugal, Spain, Italy and France; Arista et al., 2013). The cline and resulting association with abiotic forces strongly argue against pollinator mediated selection and instead point to abiotic factors which have been substantiated in a greenhouse study (Arista et al., 2013). In this species, the shift from blue to orange

(Sánchez-Cabrera et al., 2021) correlates with a biochemical transition from malvidin 3-rhamnoside to pelargonidin 3-glucoside (Harborne, 1968; Sánchez-Cabrera et al., 2021). Orange flowers have increased expression of *DFR-2*, a duplicate gene only found in orange-flowered individuals with non-synonymous SNPs suggesting substrate specificity for dihydrokaempferol drawing flux down the pelargonidin branch of the anthocyanin biosynthetic pathway (ABP) (Sánchez-Cabrera et al., 2021).

Herein, we investigate the shared blue-orange flower color polymorphism in the closely related *Lm*, a diploid perennial, that co-occurs with *La* in some populations (Figure 1). Blue flowered populations of *Lm* are more common in drier habitats of central and southwestern Iberian Peninsula and eastern North Africa; while orange-flowered populations are more often found in wetter habitats of northeastern Iberian Peninsula, western North Africa, and Sardinia (Gibbs & Talavera, 2001; Sánchez-Cabrera, 2022) (Figure 1A). In *Lm*, no populations have both color morphs (Sánchez-Cabrera, 2023). To determine the origin and maintenance of the shared blue-orange flower color variation in this species of *Lysimachia* and how it relates to the strikingly similar blue-orange flower color variation in *La*, we investigate the similarities in petal reflectance spectra, flavonoid biochemistry and compare petal transcriptomes allowing us to weigh four possible hypotheses explaining the origin and persistence of this flower color polymorphism: convergence, introgression, ancestral polymorphism or the non-monophyly of species (Figure 2).

Results

Petal UV-Vis Spectra

Reflectance spectra of petals for both species are very similar across the UV and visible wavelengths when comparing the same color morphs, yet quite different between color morphs (Figure 1B; Appendix 1—figure 1). Spectra distances between color morphs are ~7x larger than spectra distances within morphs between species (Permutational Manova, R2 = 0.75 vs. 0.15; Appendix 1—figure 1). Orange petals have double UV reflectance peaks that are absent in blue petals and differ in their primary inflection points (380, 570nm for orange and 480, 660nm for blue).

Petal Biochemical Comparisons

Biochemical analyses of petal extracts in acidified methanol using HPLC-MS-DAD revealed the underlying biochemical differences between blue and orange morphs are nearly identical between the two species. Blue petals of both species are composed of malvidin 3-rhamnoside, however small amounts of the aglycones malvidin and delphinidin, and a flavonol derivative were also detected in both species (Figure 1C; Appendix 1—table 1; Sánchez-Cabrera et al., 2021). In contrast, orange petals of both species accumulate principally pelargonidin 3-glucoside and to a lesser degree, other pelargonidin derivatives. There were no significant differences in the relative content of malvidin 3-rhamnoside and pelargonidin 3-glucoside derivatives when comparing the blue and orange samples of these two species, respectively (Figure 1C).

Transcriptome comparisons

Differential expression

Transcriptome results for *Lm* petals identified 37,552 distinct genes (see Sánchez-Cabrera et al., 2021 for *La* results including the absence of any evidence of divergent homologous copies of these genes). Of those, 336 were differentially expressed between blue and orange flowers (1.19x more genes with O > B expression; Chi-Square = 14307; p = < 2.2e-16). A total of 128 flavonoid biosynthetic pathway (FBP) genes were detected, although only five had significant differential expression, four of which had O > B expression in *Lm* (Appendix 1—table 2), three of which are in the core ABP (Figure 3C)

In comparing FBP gene expression in *Lm* to *La*, three genes (*DFR-2*, *BZ1-2* and *Caffeoyl CoA-1*) were significantly differentially expressed in both species (FDR<10^{-5} and $\log_2$FC>1; Figure 3C; Appendix 1—table 2; see Sánchez-Cabrera et al., 2021). Two key ABP genes had high expression in orange petals and were nearly undetectable in blue petals (Figure 3A, C). First, *DFR-2* with substrate specificity for pelargonidin (see references in Sánchez-Cabrera et al., 2021) had high expression in orange petals (*LmDFR-2* orange mean = 157.18; *LaDFR-2* orange mean = 99.80; Figure 3A). The second is *BZ1-2*, a gene responsible for glycosylation that stabilizes the orange pigment (*LmBZ1-2* orange mean = 2651.84; *LaBZ1-2* orange mean = 294.55; Figure 3A). However, the reciprocal decrease in expression for the primarily blue paralogue (*DFR-1* and *BZ1-1*) in orange flowers was only significant in *La*, but trends in the same

direction at similar magnitude for *LmDFR-1* (blue is ~2x higher than orange) (Figure 3A). The third gene, *Caffeoyl CoA-1*, is an early gene in the ABP that functions before the first dedicated step in the ABP (not previously reported to be involved in this type of color change; Appendix 1—figure 2B). It had higher expression in blue petals of both species and was nearly undetectable in orange petals of both species - the opposite pattern as that described above for *DFR-2* and *BZ1-2*. In addition to not having known function in the biochemistry of blue and orange, this gene is also unlikely responsible for the color change because this copy of Caffeoyl CoA has the lowest expression of the three copies expressed in petals (Appendix 1—figure 2B).

Some additional ABP genes likely involved in this color shift showed significant differential expression between colors of *La* and consistent, yet non-significant trends, in *Lm*. For example, *DFR-1* and *F3'5'H* had higher expression in blue petals than in orange petals in both species, but was only significant in *La* (2.10x and 2.45x more in *La*B and 1.80x and 4.71x more in *Lm*B, respectively; Figure 3A). Another example of an ABP gene with significant DEG in *La* and a similar trend, only significant with a Mann-Whitney U test, in *Lm* is *MYB4-2* which has higher expression in orange petals compared to blue petals (25.75x more in *La*O and 3.83x more in *Lm*O; Figure 3A). Alternatively, *CHS* showed significant differential expression between colors of *Lm*, but not significant nor consistent in *La* (1.95x more in *La*B, but 2.36x more in *Lm*O; Figure 3A) and is unlikely involved in the transition from blue to orange. Finally, a third *DFR* (*DFR-3*; Figure 4) was detected in both species, but exhibited very low expression (maximum TMM = 1.07) indicating it is not the primary gene copy at this step in the ABP in petals (*DFR-1* and *DFR-2* have >100x higher expression).

Phylogenetic analysis of ABP sequences

We compared coding sequences of a total of 22 ABP genes that were either differentially expressed in one of the species or potential candidate genes to determine whether species were monophyletic (convergence) or if color was monophyletic and transcended speciation (ancestral polymorphism). Individual phylogenetic analyses for all 22 ABP genes (10 structural and 12 regulatory) consistently recovered a monophyletic clade of *Lysimachia* samples suggesting these were broadly orthologous comparisons (>70% bootstrap support; Appendix 1—table 3 and figure 2). For two key ABP genes in the transition from blue to orange (*DFR-2* and *BZ1-2*), all orange samples

of both species are strongly supported as monophyletic (99% and 100% bootstrap, respectively; Figure 4; Appendix 1—table 3 and figure 2A). Furthermore, the regulatory locus, *bHLH12* is reciprocally monophyletic for species and within species color morphs (Appendix 1—figure 2J). In a combined phylogenetic analysis of all ABP loci, we recovered monophyletic species and monophyletic colors within each species except for paraphyletic *Lm*O (Appendix 1—figure 3).

SNP analysis

To determine if there is an association between genotype and phenotype, we examined SNPs across the FBP loci for all samples. Genes responsible for color differences in one or both species could have non-synonymous (NS) SNPs in functional regions that correlate with color within species if causal changes are in coding regions. Further, if these are shared between species this would provide further evidence supporting a single origin (ancestral polymorphism). We detected the exact same 13 NS SNPs in *DFR-2* of orange *Lm* that differentiate it from *DFR-1* which overlap with known functional regions providing substrate specificity for pelargonidin (Figure 3B) as we detected previously in *La* (see references in Sánchez-Cabrera et al., 2021).

Broadening our analysis to all FBP/ABP genes examined, only two loci have completely fixed differences between color morphs in both species (one NS SNP in *DFR-1* and two NS SNPs in *MYB4-2*; Appendix 1—table 4), but none are located in known functional sites.

By comparing NS SNPs that differentiate the color morphs with the NS SNPs that differentiate the two species, we can begin to home in on the loci responsible for the color change to begin to address if it was a single event (ancestral polymorphism or introgression) or more than one event (convergence). We find 16 NS SNPs that differentiate the two species in eight genes that we don't predict are causing the color change (Appendix 1—table 4). Noticeably absent from this list are the loci we have evidence are involved in the color shift (*DFR-1*, *DFR-2*, *BZ1-2*, *MYB 4-2*), and only one NS SNP in the extreme 5' region of *F3'5'H* (Appendix 1—table 4). Only *F3'H* showed color-specific NS SNPs, higher in *Lm* than in *La* (five vs. one), however there are even more NS SNPs between species (seven) (Appendix 1—table 4).

Structural and regulatory gene interaction

To help discern if the shared expression differences in orange petals of the two species for *DFR-2* and *BZ1-2* are controlled by the same or different regulatory genes, we looked for patterns of correlated expression with the MYB-bHLH-WD40 regulatory complex. The rationale for investigating expression correlations is that if color has evolved via independent changes in expression (i.e. developmental convergence), then we expect gene expression correlations in the gene involved to be species specific. Using a hypothesis testing approach (alpha = 0.05) in both species, *DFR-2* and *BZ1-2* were significantly positively correlated with one another (R = 0.73, p = 8.8e-05 in *La*; R = 0.62 and p = 2.9e-04 in *Lm*) and with *TTG1*, a WD40 known to activate ABP structural genes (across both genes and species p < 0.0051; Appendix 1—figure 4). Furthermore, *DFR-1* expression is negatively correlated with *MYB4-2* expression, a known repressor of ABP structural genes (R = -0.68 and p = 2.5e-04 in *La*; R = -0.62 and p = 1.4e-04 in *Lm*; Appendix 1—figure 4). *MYB4-2* is positively correlated with *DFR-2* (R = 0.39 and p = 0.37 in *La*; R = 0.47 and p = 0.0062 in *Lm*), but non-significant after Bonferroni correction.

Reproductive isolation between *La* and *Lm*

None of the crosses performed between *La* and *Lm* produced fruits irrespective of crossing direction and flower color (n=53 pollinations, see Appendix 1—table 5). In contrast, morphs within species were interfertile. Between morph crosses in *Lm* produced a mean fruit-set of 47.86 ± 0.39% (n=575) and a mean number of seeds per fruit of 16.25 ± 9.16 (n=287) (Sánchez-Cabrera, 2023) and in *La* fruit-set was 100% and the seed production was 16.95± 7.19 (n= 97) (Jiménez-López et al., 2023).

Climate niche modeling

The four morphs were statistically different from one another across most of the 19 BIOCLIM variables examined (Appendix 1—table 6). The orange and blue *La* morphs differed significantly from each other for 17 of the 19 climate variables, and the two *Lm* morphs differed for nine variables. The two orange morphs differed from one another for 16 variables and the two blue morphs differed across 11 variables.

Nine variables were significantly different between the two blue morphs and between the two orange morphs of both species. Of these, two temperature variables differed in parallel (e.g., for “isothermality” orange morphs showed lower values than blue morphs

for both species) (Appendix 1—figure 5A), while three temperature and four precipitation variables differed in opposing directions (e.g., for "annual precipitation" orange *La* were wetter than blue *La*, but orange *Lm* were drier than blue *Lm*) (Appendix 1—figure 5C).

The logistic regression results showed that the two best models using AIC did not employ any of the same variables. The best model for *La* included (in decreasing order of importance based on standardized coefficients) precipitation seasonality, isothermality and temperature seasonality, while the model for *Lm* consisted of precipitation of the wettest month and mean temperature of the wettest quarter (Appendix 1—table 7).

Since the ancestral state in *Lysimachia* is blue flowers, we hypothesized that blue would be less likely to diverge in their climate niche between the two species compared to orange morphs of the two species. We tested this with a Monte Carlo procedure that randomized colors within species and then compared observed climatic differences with differences from the null distributions. Across the 19 BIOCLIM variables, blues were more divergent between the two species than expected by chance for only one variable while orange samples were more divergent between the two species for 15 variables (~79% of variables studied), and neither color morphs were significantly different for three variables (Appendix 1—table 8).

Discussion

There are many similarities (and some differences) between color morphs of *L. arvensis* and *L. monelli* that can be used to assess the alternative hypotheses (Table 1), however definitive evidence excluding all but one of these hypotheses remains elusive. If orange evolved independently in each species (i.e. convergence; Figure 2A), we would expect distinct molecular causes (Streisfeld & Rausher, 2009; Larter et al. 2018; Ng & Smith, 2016), which we don't have any strong evidence of yet in these two species of *Lysimachia*, but the exact mutation(s) responsible for the color shift in each species awaits further genetic dissection. If the remarkably similar upregulation of *DFR-2* was activated by different MYBs in orange petals of these two species, we would expect distinct correlations in expression. Instead, *DFR-2* and *MYB4-2* are positively correlated in both species (but not significant after Bonferroni correction; Figure S5).

Alternatively, the likelihood of a single shift from blue to orange followed by introgression into the other species (Figure 2B) as clearly documented in the *Diplacus* (*Mimulus*) *aurantiacus* complex (Stankowski and Streisfeld 2015) is unlikely in *Lysimachia* for two reasons. First, although the two species co-occur, hybrids which would be morphologically distinguishable when the two species are sympatric by their flower size and overall plant size have never been found in the wild (Pujadas, 1997) unlike in the *Diplacus aurantiacus* complex where hybrid zones are well documented. Second, numerous attempted crosses of the two species reveal complete reproductive isolation (Table S7), presumable because of the ploidy differences – the members of the *Diplacus aurantiacus* complex are at least partially interfertile (Stankowski and Streisfeld 2015). But, we can only test for the likelihood of genetic exchanges between the two species in the present – there is always the possibility that there was some gene exchange soon after the (auto)poliploid speciation event. Even in that scenario, the single origin followed by introgression would require the long-term persistence of this polymorphism even though it didn't transcend the speciation event.

Given the evidence we have thus far, the most parsimonious explanation starts with a single origin - creating an ancestral polymorphism that then transcends the speciation event separating the closely related species *Lm* and *La* (Figure 2C). In this case, both blue and orange individuals would have persisted through the speciation process including polyploidy, loss of self-incompatibility, significant reduction in flower size, and a shift from perennial to annual. Although the persistence of polymorphisms across species has been documented in a few exceptional animals (see Jamie & Meier, 2020 for a review), this is the first example in plants with regards to a flower color polymorphism, however an analogous pattern of trans-specific, shared polymorphism is well documented for self-incompatibility alleles (Igić et al. 2008). Furthermore, this flower color example appears to be driven by non-pollinator agents of selection – specifically the distinct climatic niches in each species, especially those involving precipitation variables (Arista et al., 2013; Ortiz et al., 2015; Sánchez-Cabrera, 2023), yet does not appear to be maintained by negative frequency dependent selection, the most common mechanism maintaining polymorphisms over long periods of time.

A final alternative to ancestral polymorphism could involve a more complex evolutionary history where these two species are not reciprocally monophyletic

(Jiménez-López et al., 2022; Figure 2D). A source of evidence against this hypothesis is the combined phylogenetic analysis of 22 ABP loci which strongly supports the monophyly of both species (Appendix 1—figure 3). Moreover, in this scenario, a single origin of orange would have to be followed by repeated origins of polyploidy, independent losses of self-incompatibility, recurrent reduction in flower size and separate shifts to the annual habit which is substantially less parsimonious than the persistence of an ancestral polymorphism (Figure 2C vs. D).

The color morphs of these two *Lysimachia* species have nearly identical biochemical and molecular underpinnings as measured thus far. The evolution of orange pelargonidin 3-glucoside from blue malvidin 3-rhamnoside requires (1) redirecting ABP flux down the pelargonidin branch and (2) stabilizing the newly formed orange anthocyanidin with glucose instead of rhamnose. Both steps are accomplished in the same way in both species - via the recruitment of orange-specific paralogues that are undetectable in blue petals. In fact, the copy of *DFR* unique to orange petals (*DFR-2*) has nearly the same overall gene expression levels as the shared copy (*DFR-1*), but its expression is undetected in blue petals of both species. Furthermore, *DFR-2* of both species contain the same 13 NS SNPs in the substrate specificity region that differentiate it from *DFR-1*, which likely allows it to outcompete *F3'5'H* (and *F3'H*) for dihydrokaempferol thereby shunting flux down the pelargonidin branch leading to orange petals (Johnson et al., 2001; Petit et al., 2007; Katsu et al., 2017). The substantial genetic distance between *DFR-1* and *DFR-2* suggests that this duplication predated the genus and maybe even the Primulaceae family – a molecular toolkit deployed when pelargonidin provides a selective advantage. Although the exact regulatory locus (loci) responsible for these dramatic shifts in expression will require further genetic analysis, we hypothesis it involves *TTG1* (pelargonidin-specific activator) and *MYB4-2* (malvidin-specific negative regulator and potential positive activator of *DFR-2*). We find no evidence of independent NS SNPs in either *TTG1*, nor *MYB4-2*, suggesting that the polymorphism has evolved once. Instead, we see remarkably similar expression patterns and even some shared non-synonymous SNPs in both regulatory loci that are the most likely candidates for the molecular basis for this color shift.

The coordinated changes in ABP gene expression is like other blue to red flower color shifts that involve the recruitment of substrate specific *DFR* copies with correlated

downregulation of the alternative side-branch gene expression (e.g., *F3'H* and *F3'5'H*) (Zufall & Rausher, 2004; Des Marais & Rausher, 2010). We also find decreased expression in *F3'5'H* (but not *F3'H*) in orange petals of both species, however, this is only significant in *La* due to high expression variation among the blue *Lm* samples (Figure 3). Regardless, the shared expression and nearly identical coding sequences of orange *DFR-2* in *La* and *Lm* are strong evidence of a single origin that predates this speciation event and has persisted to the present in these distinct lineages.

Similarly, orange petals employ an orange-specific glycosyltransferase (*BZ1-2*), undetected in blue petals, glycosylating the orange pigment in the same way in both species. The shift from blue to orange is correlated with a dramatic increase in expression of the glycosyltransferase *BZ1-2* (similar to the *DFR*s mentioned above), which is likely involved in the stability, solubility, storage and biological activity of the anthocyanin (Yonekura-Sakakibara et al., 2008). There are no NS SNPs between orange samples of *La* and *Lm* (same evolutionary history), however two *BZ1* paralogues are highly divergent (>60% nucleotide divergence) and unalignable indicating a relatively ancient duplication event). The orange-specific *BZ1-2* of both species contains NS SNPs correlating with glucose-specificity as characterized in *Vitis vinifera* and *Medicago truncata* (He et al., 2006; Wang, 2009). In particular, there are 20 NS SNPs distinguishing these two paralogues in the PSPG-box, a conserved 44 amino acid region found in all plant UFGTs (Caputi et al., 2012) that likely confers glucose-specificity of *BZ1-2*. We infer that the two paralogues likely have different functions regarding which sugar they add and their efficiency in doing so (Sun et al., 2016), but within a color morph for both species, their sequence similarity suggest they perform the same function. In contrast to *BZ1-2*, *BZ1-1* has variable expression in both color morphs - *La* has significantly higher expression in blue than orange as expected, but mean expression is similar in blue and orange *Lm* (and not significant). Regardless of whether there is compensatory downregulation in orange petals of *BZ1-1*, we know that *BZ1-2* has 10-50x higher expression in orange and we predict that it has higher efficiency in adding glucose to pelargonidin of orange petals than *BZ1-1* (Sun et al., 2016). Although there are other examples of closely related species exhibiting the same flower color because they accumulated similar major categories of anthocyanidins (i.e. aglycones) (e.g. Ng & Smith, 2016; Larter et al., 2018; Ogutcen et al., 2020), the specific

anthocyanins they accumulate are generally distinct due to the enormous diversity of chemical decorations in the flavonoids (Passeri et al., 2016; Berardi et al., 2021). In these two *Lysimachia* species, orange morphs use the same *3GT* correlated with the predominant glycosylation of pelargonidin clearly indicating a single ancestral evolutionary transition shared by both species that has transcended the speciation event.

If *DFR-2* and *BZ1-2* are similarly upregulated in orange *La* and *Lm*, we predict they will be controlled by the same regulatory gene(s) in both species if there was a single ancestral polymorphism. In fact, expression of *DFR-2* and *BZ1-2* in orange petals of both species is positively correlated with the same regulatory gene *TTG1* (WD40) known to control these two ABP structural genes (Tiang & Wang, 2020) (Appendix 1—figure 4). Looking at the sequence of this regulatory gene, there is only one color differentiating NS SNP in *La* and none in *Lm* strongly suggesting another trans-acting regulatory gene is likely responsible for the differential expression of *TTG1* in blue and orange morphs of these two *Lysimachia* species. However, *MYB4-2* has two NS SNPs shared by both species that positively correlates with *DFR-2* expression (Appendix 1—figure 4).

For both *Lysimachia* species, *DFR-1* expression in orange petals is negatively correlated with *MYB4-2* expression (Appendix 1—figure 4). Moreover, in *La* this increase of *MYB4-2* is correlated with a decrease in *F3'5'H* in orange petals, facilitating the redirection of ABP flux to the pelargonidin branch of the pathway. Although *MYB4-2* has low expression in both morphs of *Lm* and is not significantly correlated with *DFR-1* nor *F3'5'H*, it exhibited significant differential expression between morphs (Mann-Whitney U test, $U = 19$, $p = 0.021$). In *Arabidopsis thaliana* and *Vitis vinifera*, *MYB4* represses anthocyanin biosynthesis either through direct binding to the promoter regions of ABP genes (*ANS*, *DFR* and *UFGT*) or by displacing the activator MYB in the MBW complex (Pérez-Díaz et al., 2016; Chen et al., 2019). However, how could *MYB4-2* repress *DFR-1* and not *DFR-2*? Like in *Lotus* (Yoshida et al., 2010) and *Fagopyrum* (Katsu et al., 2017) where different *DFR* paralogues are independently regulated by their unique promoter sequences, we predict that *MYB4-2* has differential regulatory effects on the two primary *DFR* paralogues. Overall, we argue that *MYB4-2* contributes to redirecting ABP flux down the pelargonidin branch of the pathway by negatively

regulating the non-orange-specific paralogues at the critical branchpoint (*DFR-1* and *F3'5'H*) in both species similarly.

Previous experimental work and our climate niche modelling indicate that there may be pleiotropic effects of petal color. Orange morphs of both species are found in locations with colder winters than blue morphs (Appendix 1—figure 5A). However, the two morphs appear to respond in opposing directions to primarily moisture-related climate niche variables (Appendix 1—figure 5C). Orange *Lm* is found in habitats with a wide range of precipitation while orange *La* is found in wet habitats. Although the climate niche of the blue morphs of the two species are often distinct, the orange samples are clearly driving these orthogonal responses to precipitation. Why a biochemically and genetically similar polymorphism shared between different species would have contrasting ecological side-effects remains unclear. Previous experimental work in *La* shows that blue-flowered individuals (containing rhamnose stabilized malvidin) inhabit environments with lower precipitation and higher solar radiation than orange-flowered plants with glucose-bound pelargonidin, potentially linking abiotic stress with differential glycosylation (Arista et al., 2013; Sánchez-Cabrera, 2022). If *BZ1-2* is only found in orange petals and is glucose-specific, then does the type of sugar confer physiological or ecologically-relevant adaptations in *Lysimachia*? The coupling of rhamnose to malvidin found in *Lysimachia* also explains the blue color of *Petunia hybrida* (Kroon et al., 1994), *Lobelia erinus* (Hsu et al., 2017) and *Parochetus communis* (Tatsuzawa, 2020) and is known to provide stress tolerance (e.g. UV response) when rhamnose is bound to flavonoids (Li et al., 2017; Jiang et al., 2021). However, in *Lm*, the opposite is true for several climate niche parameters, especially with regard to precipitation (Appendix 1—table 7 and figure 5C). It appears this shared color polymorphism that may have transcended speciation confers unique climate niches.

Further evidence of gene function, enzyme kinetics and genetic association must be conducted before any final conclusions can be made regarding the molecular causes and ecological consequences of this flower color variation. However, the data presented herein lean toward a single biochemical and molecular footprint shared by both species. If the shift from blue to orange happened twice (i.e. convergence), it would be remarkable since it would most likely be in the same trans-acting regulator of *TTG1*.

Additional experimental approaches (genetic dissection, transformation, knock-out, *DFR* specificity enzyme assays, etc.) promise to identify the type, number and order of mutations responsible for these flower color changes, yet given the phenotypic, biochemical and transcriptome similarities described here, we have yet to find any strong evidence rejecting the ancestral polymorphism hypothesis.

Methods

Population sampling

We collected stem cuttings from blue-flowered populations from southern Spain (seven of *Lm* and one of *La*) and from orange-flowered populations from northern Spain, Morocco and Italy (five of *Lm* and one of *La*) (Appendix 1—table 9). Cuttings were rooted in an aeroponic cloner under glasshouse conditions. We also sowed seeds from blue-flowered plants from Portugal in glasshouses at the University of Seville. Voucher specimens were deposited in the University of Seville Herbarium (SEV, Appendix 1—table 9).

We sampled all five petals per flower from a mean of 19 flowers per plant (10 - 24 flowers) from ten blue- and ten orange-flowered plants of *Lm*, and a mean of 30 flowers per plant from eight flowered plants of each color in *La* (see Sánchez-Cabrera et al. (2021) for more details on *La* sampling). In all cases the bullseye at the petal base was avoided. All samples were taken from first-day anthesis flowers and immediately, petals were flash frozen and stored at -80ºC. For flavonoid profiling, we collected 10 samples per flower color for *Lm* (flowers from different plants of the same population per sample), including those present in the RNA-Seq analysis (Appendix 1—table 9). *La* samples were obtained from 14 blue- and 11 orange-flowered individuals (see Sánchez-Cabrera et al. 2021). For both species, each sample consisted of two to five flowers without the bullseye.

UV-Vis petal spectra

Reflectance spectra of the adaxial surface of 44 blue and 67 orange petals of *La* and 75 blue and 50 orange petals of *Lm* were captured using a JAZ A1465 double-beam spectrophotometer (Ocean Optics, Florida, USA). The deuterium-tungsten light source provided reflectance between 300 and 700 nm.

We tested the UV-vis spectra for the relative amounts of variation in two tests (1) between color morphs within a species versus (2) between species within a color morph using permutational multivariate analysis (PERMANOVA test) (Maia & White, 2018). For each test, we computed the Euclidean distances based on the difference in reflectance at each wavelength between all pairs of individual spectra and conducted permutational MANOVA tests (Anderson, 2001) to assess statistical differences (9999 permutations) making quantitative comparative statements between the R^2 values of the two tests (adonis2 in vegan in R). We visualized the distances between the spectra using metaMDS in vegan in R with 500 tries.

Identification of flavonoid compounds

Flavonoids were extracted by placing petal samples (see Population sampling section; Appendix 1—table 9) in microtubes containing 500µl of MeOH with 1% HCl and stored at -80°C. Homogenization was performed with a BeadBeater using 3 x 3.2 mm steel balls for 30 seconds, then centrifuged for 10 min to pellet cellular debris. Samples of the supernatant were loaded on a Dionex UltiMate3000 ultra-high pressure liquid chromatography system equipped with a diode array detector and connected to a Thermo Fleet LCQ mass spectrometer (Thermo-Fisher, Waltham, MA USA). Data were analyzed using Xcalibur software (Thermo Fisher Scientific). Flavonoid identification was based on the compound's retention time, UV-Vis spectra and whenever possible, chromatographic comparisons with authentic standards: quercetin, luteolin, kaempferol, isorhamnetin, malvidin, pelargonidin, cyanidin and delphinidin (Extrasynthese, Genay, France), previously reported for other *Lysimachia* species (see Sánchez-Cabrera et al., 2021). Relative contents (%) of the primary anthocyanins of each color morph sample, based on the total area under the curve, were calculated and used in statistical comparisons between the two species applying a Mann-Whitney U test in R.

RNA extraction and reads filtering

Collected petals (see Population sampling section) were homogenized using a mortar and pestle. Total RNA was then extracted following the Qiagen RNeasy Plant Mini Kit protocol (Qiagen, Germany) with the addition of PEG 20,000 mol. wt. (550µl, 2%; Gehrig et al. 2000) before the first filtering step. The addition of PEG was essential to achieve reasonable RNA concentrations for library preparation and sequencing. RNA

samples were stored at -80ºC until further analysis. RNA concentration and purity was initially assessed with a Nanodrop Nd-1000 (ThermoFisher) and agarose gel, and then confirmed with a Bioanalyzer (Agilent, Santa Clara, CA, USA) before sequencing. Individual libraries were barcoded, multiplexed and sequenced as 150 bp paired-end reads using two lanes on an Illumina Hi-Seq 2000 (Illumina, San Diego, CA, USA) through Novogene (Beijing, China). Raw paired-end Illumina reads were assessed for quality using FastQC (Andrews, 2010) and were processed using Rcorrector v1.0.4 (Song and Florea, 2015) to correct random sequencing errors. Then, reads were trimmed with Trimmomatic v0.39 (Bolger et al., 2014) to remove any read containing bases with Phred scores lower than 20, low quality reads less than 50 bp long, and any adapter or other Illumina-specific sequences that were still present (Appendix 1—table 10).

Identification of differentially expressed genes (DEGs)

To determine DEGs for *Lm*, we used the *La* transcriptome assembly with known ABP genes identified (Sánchez-Cabrera et al., 2021) as reference for mapping *Lm* RNA-Seq samples with Bowtie2 software (Langmead & Salzberg, 2012). We calculated Trimmed mean of M-values (TMM, mean of log-expression ratios; Robinson & Oshlack, 2010) for each gene using RSEM software (Li & Dewey, 2011). Then, with EdgeR package (Robinson et al., 2009) in R v4.0.0 (R Core Team, 2020) we determined statistically significant differentially expressed genes (DEGs) between blue and orange petal samples, applying the conservative thresholds for DEG identification: the false discovery rate (FDR) less than 10^{-5} and the expression difference threshold was greater than one $\log_2$ fold-change ($\log_2$FC), following Sánchez-Cabrera et al. (2021). To keep biologically interesting genes for differential expression analysis, we considered those genes with more than one count per million (CPM) in a minimum of four samples. Some regulatory genes have very low expressions and magnitudes were unreliable. For those loci, we performed the non-parametric Mann-Whitney U test to test for differential expression.

Genes and isotigs selection for analysis and correlated expression analysis

We selected 22 ABP color differentiating structural and regulatory genes with differential expression between colors in either both species, just in one species or not differentially expressed but was a copy of a DEG (see Results section). We established

a criterion to select one isotig per gene: (1) samples with less than 20% non-identified nucleotides in the CDS, (2) samples with more than 100 reads mapping to the sequence, (3) samples with longest CDS, (4) samples with higher expression. Finally, we selected the isotig which was present in a higher number of samples after applying the criteria. We tested for correlated expression among the 22 structural and regulatory genes in both species using Kendall correlations with Bonferroni correction for multiple testing in R.

Phylogenetic analyses and non-synonymous SNP identification

We conducted phylogenetic analyses on the selected isotigs for all ABP structural and regulatory genes. We followed the methods described in Sánchez-Cabrera et al. (2021) to map to reference the reads using Geneious v9.0.4 (Kearse et al., 2012). For the outgroups, we used top BLASTn hits (filtering for *Cyclamen* sp., *Camellia* sp., *Vaccinium* sp., *Actinidia* sp. and *Rhododendron* sp. when available) and, when possible, top tBLASTx from *Camellia sinensis*, *Embelia ribes* and *Primula veris* genomes. We reconstructed the relationships using the RAxML 7.2.8 plug-in from within Geneious v9.0.4, searching for the maximum likelihood tree with 1000 bootstrap replicates. We added normalized expression values (TMM) to the phylogenetic trees with "ggtree" (Yu et al., 2017) and "phytools" (Revell, 2012) packages in R v4.0.0 (R Core Team, 2020). We concatenated alignments of all ABP structural and regulatory loci and performed a combined phylogenetic analysis using the same methodology as above but partitioning the data by locus and determining the best fit model of nucleotide substitution.

We calculated the NS SNP rate between blue and orange petals of each species, with a cutoff of 75% difference between colors. We used the isotigs selected for NS SNP search. We focused on genes with orange monophyly to either one or both species, because orange is derived from blue and therefore, we expect genes responsible for the blue to orange shift to show a single common ancestor for the orange samples.

Differentiating the four hypotheses

To differentiate the four hypotheses (Figure 2) we used the following logic. First, the convergence hypothesis predicts separate origins of the blue to orange color shift which would produce separate clades of orange samples for both species. Under this hypothesis, and with enough data, *La* and *Lm* should be reciprocally-monophyletic. The

introgression hypothesis involves a single origin of the color change in both species (after the speciation event) which would appear as very close relationships for the color differentiating locus between orange *Lm* and *La* since they are the same gene, just shared across species boundaries (for the color causing gene(s) the species should not be monophyletic), yet for non-color causing loci, species may be monophyletic. However, the species must be interfertile. Third, the ancestral polymorphism hypothesis produces a single origin of the color change (before the speciation event) creating separate monophyletic blue and orange clades. Finally, if taxonomic confusion has blurred the identity of the species (non-monophyletic species hypothesis, Jiménez-López et al., 2022), then there could be a monophyletic color clade (across species boundaries) – a topology expected for all loci, not just those contributing to the color shift.

Reproductive isolation between La and Lm

To determine reproductive isolation between *La* and *Lm*, we performed controlled crosses in plants from different populations grown in glasshouse. Flowers were emasculated before anthesis, and hand-pollinations were made during the first day of anthesis within and between species and color morphs. Pollinated flowers were left to set fruits and the fruit production and the number of seeds per fruit were counted.

Climate niche modeling

To test whether the color morphs of each species differed ecologically across their ranges, we constructed an occurrence dataset using a combination of personal observations and iNaturalist (inaturalist.org) records (manually verified for species identification and color; Appendix 1—figure 6). The dataset comprised 4287 records. All 19 BIOCLIM variables were then extracted for each record based on GPS coordinates at the highest available spatial resolution (30 second) (Fick and Hijmans, 2017). Occurrences with no climate data and duplicated occurrences (multiple occurrences of the same species with the same flower color within a pixel) were deleted. There were 3309 occurrences in the final dataset (*La* blue = 641, *La* orange = 1941, *Lm* blue = 662, *Lm* orange = 65).

To test for univariate climatic differences among the four morphs, a separate Kruskall-Wallis test with a post-hoc Dunn test (non-parametric analogs of ANOVA with post-hoc Tukey's test) was applied to each variable. Significance tests used Bonferroni

adjustment for 76 comparisons (19 climate variables across four species/flower color combinations).

To determine whether similar climate variables were most important for separating color morphs in the two species, logistic regression models were built for each species on a subset on non-correlated climate variables. First, strongly correlated climate variables were removed and a dataset of five variables that were both relatively uncorrelated and putatively biologically meaningful based on field observations and experimental manipulations (Arista et al. 2013; J. Jiménez-Lopez et al., unpublished data) were retained: precipitation of wettest month, precipitation seasonality, isothermality, temperature seasonality and mean temperature of wettest quarter. Data were normalized using the ‘normalize’ procedure in the ‘decostand’ function from the vegan R package (Oksanen et al. 2019) to facilitate later comparison of regression coefficients. Best fit models were selected using AIC scores derived from the ‘dredge’ function from the MuMIn R package (Bartón, 2020).

To test whether the two orange morphs were more divergent than the two blue morphs across the 19 BIOCLIM variables, a randomization procedure was used. The specific null hypothesis was no difference between the distance between the two orange morph means and the distance between the two blue morph means. To build a null model for each of the 19 variables, species identities were retained but color morphs were randomized 999 times. For each distribution, one tail indicated that differences between orange populations was greater while the other tail indicated greater differences between blue populations. A two-tailed test indicated whether observed orange differences were greater than expected, whether blue differences were greater than expected or whether neither color was more divergent.

Data Availability

The data that support the findings of this study are openly available in Genbank (raw reads & assembled contigs) and Figshare (spectra, biochemistry, expression values, alignments).

Raw reads, assembled contigs and expression values will be made available from Genbank and FigShare. R scripts to conduct statistical analyses will also be available from FigShare.

Acknowledgements

We would like to thank the support staff in the Department of Biology and the Department of Chemistry and Biochemistry at Santa Clara University. Boris Igić provided thoughtful insights on the evolutionary history of color in these species. We would like to thank M. Abdelaziz for his help in organizing the field collecting trip and during the sampling of Moroccan *L. monelli* plants. Grants PID2020-116222GB-100 to M.A. and E.N., CGL2015-63827 to M.A. and P.L.O. and BES-C-2016-0023 to M.S.C funded by MCIN/AEI/ 10.13039/501100011033 and by "European Union NextGenerationEU/PRTR".

Conflict of interest

None

Author contributions

MS-C, EN, MA, PO, and JW designed and performed research; AF conducted the UHPLC technique; BC conducted the climate niche analyses; FJ-L performed plant crosses and supplied *L. arvensis* reflectance data. MS-C, EN, and JW analyzed data; and MS-C and JW wrote and revised the paper with assistance from coauthors.

References

Allison AC. 1961. Genetic factors in resistance to malaria. *Ann. N. Y. Acad. Sci.* **91**: 710–729.

Anderson MJ. 2001. A new method for non-parametric multivariate analysis of variance. *Austral Ecol.* **26**: 32–46.

Arista M, Talavera M, Berjano R, Ortiz PL. 2013. Abiotic factors may explain the geographical distribution of flower colour morphs and the maintenance of colour polymorphism in the scarlet pimpernel. *J. Ecol.* **101**: 1613–1622.

Bartón K. 2020. *MuMIn: Multi-Model Inference.* R package version 1.43.17.

Berardi AE, Esfeld K, Jäggi L, Mandel T, Cannarozzi GM, Kuhlemeier C. 2021. Complex evolution of novel red floral color in *Petunia*. *Plant Cell* 33: 2273–2295.

Caputi L, Malnoy M, Goremykin V, Nikiforova S, Martens S. 2012. A genome-wide phylogenetic reconstruction of family 1 UDP-glycosyltransferases revealed the

expansion of the family during the adaptation of plants to life on land. *Plant J.* **69**: 1030–1042.

Chen C, Zhang K, Khurshid M, Li J, He M, et al. 2019. MYB transcription repressors regulate plant secondary metabolism. *Crit. Rev. Plant Sci.* **38**: 159–170.

Comeault AA, Flaxman SM, Riesch R, et al. 2015. Selection on a genetic polymorphism counteracts ecological speciation in a stick insect. *Curr. Biol.* **25**: 1975–1981.

Conway MS. 2005. *Life's solution: inevitable humans in a lonely universe*. Cambridge, UK: Cambridge University Press.

Corl A, Davies AR, Kuchta SR, Sinervo B. 2010. Selective loss of polymorphic mating types is associated with rapid phenotypic evolution during morphic speciation. *Proc. Natl. Acad. Sci. U.S.A.* **107**: 4254–4259.

Des Marais DL, Rausher MD. 2010. Parallel evolution at multiple levels in the origin of hummingbird pollinated flowers in *Ipomoea*. *Evolution* **64**: 2044–2054.

Dobzhansky T. 1937. *Genetics and the origin of species*. New York, NY: Columbia University Press.

Fick SE, Hijmans RJ. 2017. WorldClim 2: new 1km spatial resolution climate surfaces for global land areas. *Inter. J. Climat*. **37**: 4302–4315.

Gibbs PE, Talavera S. 2001. Breeding system studies with three species of *Anagallis* (Primulaceae): self-incompatibility and reduced female fertility in *A. monelli* L. *Ann. Bot.* **88**: 139–144.

Gould SJ. 1989. *Wonderful life: the Burgess shale and the nature of history*. New York, NY: W.W. Norton.

Grant V. 1981. *Plant speciation*, 2nd ed. New York, NY: Columbia University Press.

Harborne JB. 1968. Comparative biochemistry of the flavonoids. VII. Correlations between flavonoid pigmentation and systematics in the family Primulaceae. *Phytochemistry* **7**: 1215–1230.

He XZ, Wang X, Dixon RA. 2006. Mutational analysis of the *Medicago* glycosyltransferase UGT71G1 reveals residues that control regioselectivity for (iso)flavonoid glycosylation. *J. Biol. Chem.* **281**: 34441–34447.

Hsu YH, Tagami T, Matsunaga K, Okuyama M, Suzuki T, et al. 2017. Functional characterization of UDP-rhamnose-dependent rhamnosyltransferase involved in

anthocyanin modification, a key enzyme determining blue coloration in *Lobelia erinus*. *Plant J.* **89**: 325–337.

Hugall AF, Stuart-Fox D. 2012. Accelerated speciation in colour-polymorphic birds. *Nature* **485**: 631–634

Igić B, Kohn JR. 2001. Evolutionary relationships among self-incompatibility RNases. *Proc. Natl. Acad. Sci. U.S.A.* **98**: 13167–13171.

Igić B, Lande R, Kohn JR. 2008. Loss of self-incompatibility and its evolutionary consequences. *Int. J. Plant Sci.* **169**: 93–104.

Jamie GA, Meier JI. 2020. The persistence of polymorphisms across species radiations. *Trends Ecol. Evol.* **35**: 795–808.

Jiang N, Dillon FM, Silva A, Gomez-Cano L, Grotewold E. 2021. Rhamnose in plants-from biosynthesis to diverse functions. *Plant Sci.* **302**: 110687.

Jiménez-López FJ, Matas L, Arista M, Ortiz PL. 2019. Flower colour segregation and flower discrimination under the bee vision model in the polymorphic *Lysimachia arvensis*. *Plant Biosyst.* **154**: 535–543.

Jiménez-López FJ, Viruel J, Arista M, Ortiz PL, Talavera M. 2022. Molecular approaches reveal speciation between red- and blue-flowered plants in the Mediterranean *Lysimachia arvensis* and *L. monelli* (Primulaceae). *Bot. J. Linn. Soc.* **199**: 557–577.

Jiménez-López FJ, Arista M, Talavera M, Morellato LP, Pannell JR, Viruel J, Ortiz PL. 2023. Multiple pre- and post-zygotic componets of reproductive isolation between two co-occurring *Lysimachia* species. *New Phytol.* **238**: 874–887.

Johnson ET, Ryu S, Yi HK, Shin B, Cheong H, Choi G. 2001. Alteration of a single amino acid changes the substrate specificity of dihydroflavonol 4-reductase. *Plant J.* **25**: 325–333.

Katsu K, Suzuki R, Tsuchiya W, Inagaki N, Yamazaki T, et al. 2017. A new buckwheat dihydroflavonol 4-reductase (DFR), with a unique substrate binding structure, has altered substrate specificity. *BMC Plant Biol.* **17**: 1–14.

Kroon J, Souer E, De Graaff A, Xue Y, Mol J, Koes R. 1994. Cloning and structural analysis of the anthocyanin pigmentation locus Rt of *Petunia hybrida*: characterization of insertion sequences in two mutant alleles. *Plant J.* **5**: 69–80.

Larter M, Dunbar-Wallis A, Berardi AE, Smith SD. 2018. Convergent evolution at the pathway level: predictable regulatory changes during flower color transitions. *Mol. Biol. Evol.* **35**: 2159–2169.

Li P, Li YJ, Zhang FJ, Zhang GZ, Jiang XY, et al. 2017. The *Arabidopsis* UDP-glycosyltransferases UGT79B2 and UGT79B3, contribute to cold, salt and drought stress tolerance via modulating anthocyanin accumulation. *Plant J.* **89**: 85–103.

Madsen T, Stille B, Ujvari B, Bauwens D, Endler JA, 2022. Negative frequency-dependent selection on polymorphic color morphs in adders. *Curr. Biol*. **32**: 3385–3388.

Maia R, White TE. 2018. Comparing colors using visual models. *Behav. Ecol.* **29**: 649–659

Mallet J. 2005. Hybridization as an invasion of the genome. *Trends Ecol. Evol.* **20**: 229–237.

Martin SH, Dasmahapatra KK, Nadeau NJ, Salazar C, Walters JR, et al. 2013. Genome-wide evidence for speciation with gene flow in *Heliconius* butterflies. *Genome Res.* **23**: 1817–1828.

McKinnon JS, Pierotti ME. 2010. Colour polymorphism and correlated characters: genetic mechanisms and evolution. *Mol. Ecol.* **19**: 5101–5125.

McLean CA, Stuart-Fox D. 2014. Geographic variation in animal colour polymorphisms and its role in speciation. *Biol. Rev.* **89**: 860–873.

McRobie HR, Moncrief ND, Mundy, NI. 2019. Multiple origins of melanism in two species of North American tree squirrel (*Sciurus*). *BMC Evol. Biol.* **19**: 1–14.

Monein A, Atta II, Shehata AA. 2003. On the delimitation of *Anagallis arvensis* L. (Primulaceae) 1. Evidence based on micromorphological characters, palynological features and karyological studies. *Pakistan J. Biol. Sci.* **6**: 29–35.

Muchhala N, Johnsen S, Smith, SD. 2014. Competition for hummingbird pollination shapes flower color variation in Andean Solanaceae. *Evolution* **68**: 2275–2286.

Ng J, Smith SD. 2016. How to make a red flower: the combinatorial effect of pigments. *AoB Plants* 8: plw013.

Nolte AW, Gompert Z, Buerkle CA. 2009. Variable patterns of introgression in two sculpin hybrid zones suggest that genomic isolation differs among populations, *Mol. Ecol.* **18**: 2615–2627.

Ogutcen E, Durand K, Wolowski M, Clavijo L, Graham C, Glauser G, Perret M. 2020. Chemical basis of floral color signals in Gesneriaceae: the effect of alternative anthocyanin pathways. *Front. Plant Sci*. **11**: 604389.

Oksanen J, Blanchet FG, Friendly M, Kindt R, Legendre P, et al. 2019. *vegan: community ecology package*. R package version 2.5-6. https://CRAN.R-project.org/package=vegan

Ortiz PL, Berjano R, Talavera M, Rodríguez-Zayas L, Arista M. 2015. Flower colour polymorphism in *Lysimachia arvensis*: how is the red morph maintained in Mediterranean environments? *Perspect. Plant Ecol. Evol. Syst.* **17**: 142–150.

Passeri V, Koes R, Quattrocchio FM. 2016. New challenges for the design of high value plant products: stabilization of anthocyanins in plant vacuoles. *Front. Plant Sci*. **7**: 153.

Petit P, Granier T, d' Estaintot BL, Manigand C, Bathany K, Schmitter JM, et al. 2007. Crystal structure of grape dihydroflavonol 4-reductase, a key enzyme in flavonoid biosynthesis. *J. Mol. Biol*. **368**: 1345–1357.

Pérez-Díaz JR, Pérez-Díaz J, Madrid-Espinoza J, González-Villanueva E, Moreno Y, Ruiz-Lara S. 2016. New member of the R2R3-MYB transcription factors family in grapevine suppresses the anthocyanin accumulation in the flowers of transgenic tobacco. *Plant Mol. Biol.* **90**: 63–76.

Pujadas A. 1997. *Anagallis* L. In: Castroviejo S, Aedo C, Laínz M, Morales R, Muñoz Garmendia F, et al., eds. *Flora Iberica, V. Ebenaceae-Saxifragaceae*. Madrid, Spain: Real Jardín Botánico, CSIC, 57–62.

Revell LJ. 2012. phytools: An R package for phylogenetic comparative biology (and other things). *Methods Ecol. Evol.* **3**: 217–223.

Sánchez-Cabrera M. 2023. *Flower color polymorphism and speciation: Lysimachia monelli and Lysimachia arvensis as study systems.* Ph.D. thesis, University of Seville, Seville, Spain.

Sánchez-Cabrera M, Jiménez-López FJ, Narbona E, Arista M, Ortiz PL, Romero-Campero FJ, et al. 2021. Changes at a critical branchpoint in the anthocyanin biosynthetic pathway underlie the blue to orange flower color transition in *Lysimachia arvensis*. *Front. Plant Sci.* **12**: 247.

Schemske DW, Bierzychudek P. 2007. Spatial differentiation for flower color in the desert annual *Linanthus parryae*: was Wright right? *Evolution* **61**: 2528–2543.

Sirugo G, Predazzi IM, Bartlett J, Tacconelli A, Walther M, Williams SM. 2014. G6PD A-deficiency and severe malaria in The Gambia: heterozygote advantage and possible homozygote disadvantage. *Am. J. Trop. Med. Hyg.* **90**: 856.

Stankowski S, Streisfeld MA. 2015. Introgressive hybridization facilitates adaptive divergence in a recent radiation of monkeyflowers. *Proceedings of the Royal Society B: Biological Sciences.* **282**: 20151666.

Streisfeld MA, Rausher MD. 2009. Genetic changes contributing to the parallel evolution of red floral pigmentation among *Ipomoea* species. *New Phytol.* **183**: 751–763.

Sun W, Liang L, Meng X, Li Y, Gao F, Liu X, et al. 2016. Biochemical and molecular characterization of a flavonoid 3-O-glycosyltransferase responsible for anthocyanins and flavonols biosynthesis in *Freesia hybrida*. *Front. Plant Sci.* **7**: 410.

Svensson EI. 2017. Back to basics: using colour polymorphisms to study evolutionary processes. *Mol. Evol.* **26**: 2204–2211.

Tatsuzawa F. 2020. Flavonoids in the blue flowers of *Parochetus communis* Buch.-Ham. ex D. Don (Leguminosae). *Biochem. Syst. Ecol.* **92**: 104–108.

Thomson JD, Wilson P. 2008. Explaining evolutionary shifts between bee and hummingbird pollination: convergence, divergence, and directionality. *Int. J. Plant Sci.* **169**: 23–38.

Tian H, Wang S. 2020. TRANSPARENT TESTA GLABRA1, a key regulator in plants with multiple roles and multiple function mechanisms. *Int. J. Mol. Sci.* **21**: 4881.

Wang X. 2009. Structure, mechanism and engineering of plant natural product glycosyltransferases. *FEBS Lett.* **583**: 3303–3309.

Wessinger CA, Rausher MD, Hileman LC. 2019 Adaptation to hummingbird pollination is associated with reduced diversification in *Penstemon*. *Evol. Lett.* **3**: 521–533.

Wessinger CA, Rausher MD. 2013. Predictability and irreversibility of genetic changes associated with flower color evolution in *Penstemon barbatus*. *Evolution* **68**: 1058–1070.

Wright S. 1943. An analysis of local variability of flower color in *Linanthus parryae.* *Genetics* **28**: 139–156.

Yonekura-Sakakibara K, Nakayama T, Yamazaki M, Saito K. 2008. Modification and stabilization of anthocyanins. In: Winefield C, Davies K, Gould K, eds. *Anthocyanins*. New York, NY: Springer.

Yoshida K, Iwasaka R, Shimada N, Ayabe S, Aoki T, Sakuta M. 2010. Transcriptional control of the dihydroflavonol 4-reductase multigene family in *Lotus japonicus*. *J. Plant Res.* **123**: 801–805.

Yu G, Smith D, Zhu H, Guan Y, Lam TT. 2017. ggtree: an R package for visualization and annotation of phylogenetic trees with their covariates and other associated data. *Methods Ecol. Evol.* **8**: 28–36.

Zufall RA, Rausher MD. 2004. Genetic changes associated with floral adaptation restrict future evolutionary potential. *Nature* **428**: 847–850.

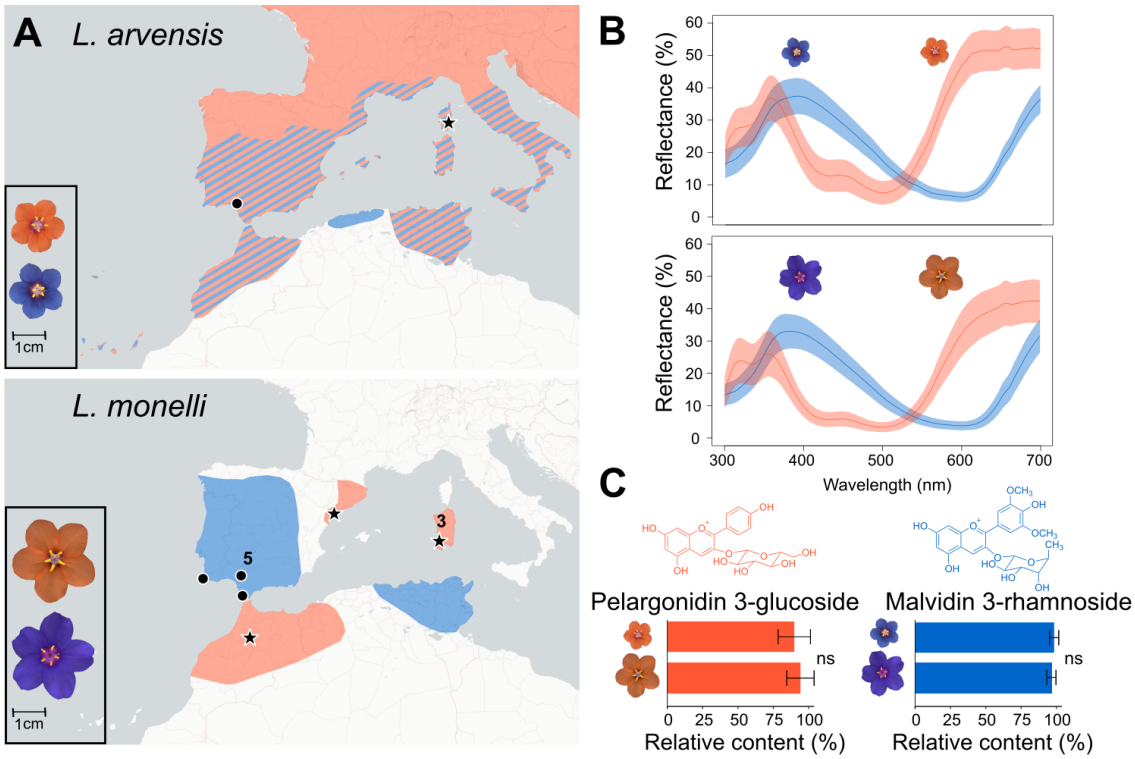

Figure 1. Flower color characterization of blue and orange *Lysimachia arvensis* and *L. monelli*. (A) Scaled images and geographic distributions of the two flower color morphs of both species. Coexistence of the *L. arvensis* color morphs is indicated with diagonal striping. Populations sampled for transcriptome comparisons are indicated with black circles (blue) and black stars (orange) (numbers indicate >1 geographically adjacent populations were sampled for *L. monelli*). (B) UV-vis reflectance spectra of blue and orange petals of both species showing mean curves with 95% confidence intervals in colored shading above and below the mean curve. (C) Molecular structures and relative content from the biochemical analysis of the primary anthocyanins in both species. Non-significant differences (ns) in relative content are indicated using a Mann-Whitney U test. In *L. arvensis*, orange samples include pelargonidin 3-glucoside derivatives. Error bars represent standard error (SEM).

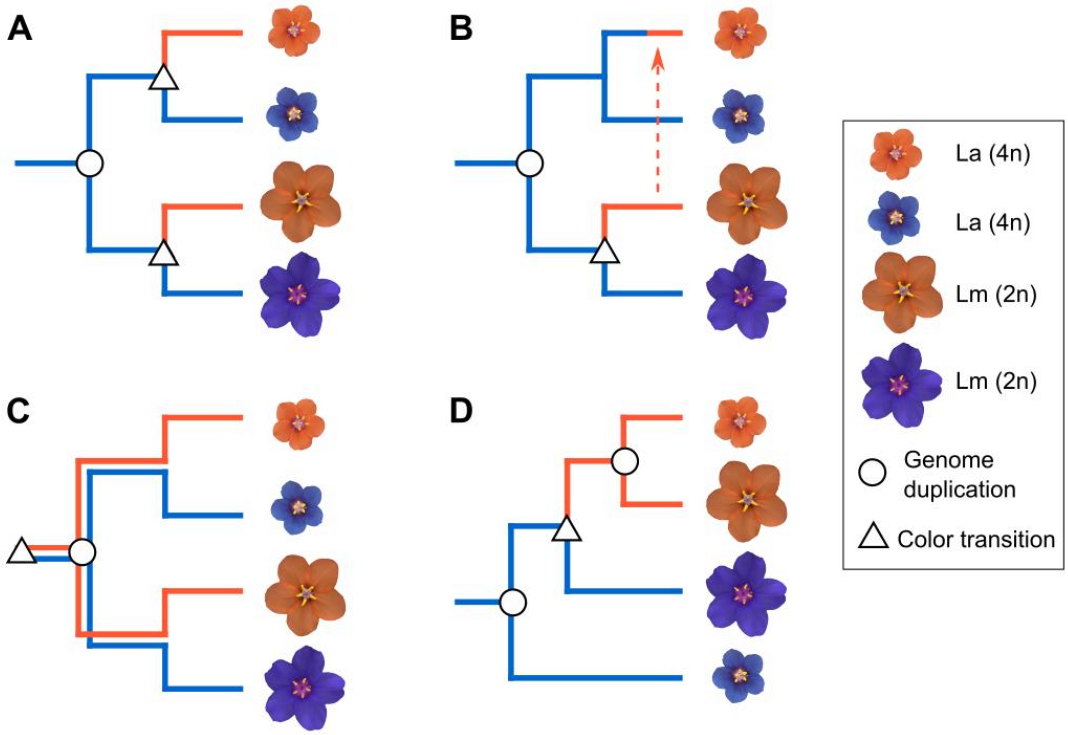

Figure 2. Four evolutionary hypotheses of petal color evolution in *L. arvensis* and *L. monelli*. Assuming the ancestral state is blue and diploid, the most parsimonious color shifts are indicated by a triangle and ploidy changes are indicated with a circle (placed at the node since they likely drive divergence). In (A), convergent evolution of orange petals is coupled with a single origin of the tetraploid lineage predicts independent and distinct molecular causes for the color change in each lineage. In (B), a single origin of orange petals in *L. monelli* followed by introgression to *L. arvensis* requires only one shift to orange and one polyploid event but requires the lineages to be able to hybridize. In (C), a single origin of orange in the common ancestor creates an ancestral polymorphism that transcends the speciation event and persists to the present in both species, requiring one polyploidy event. In (D), non-monophyletic species allow for a single origin of orange petals but requires independent origins of the tetraploid lineages.

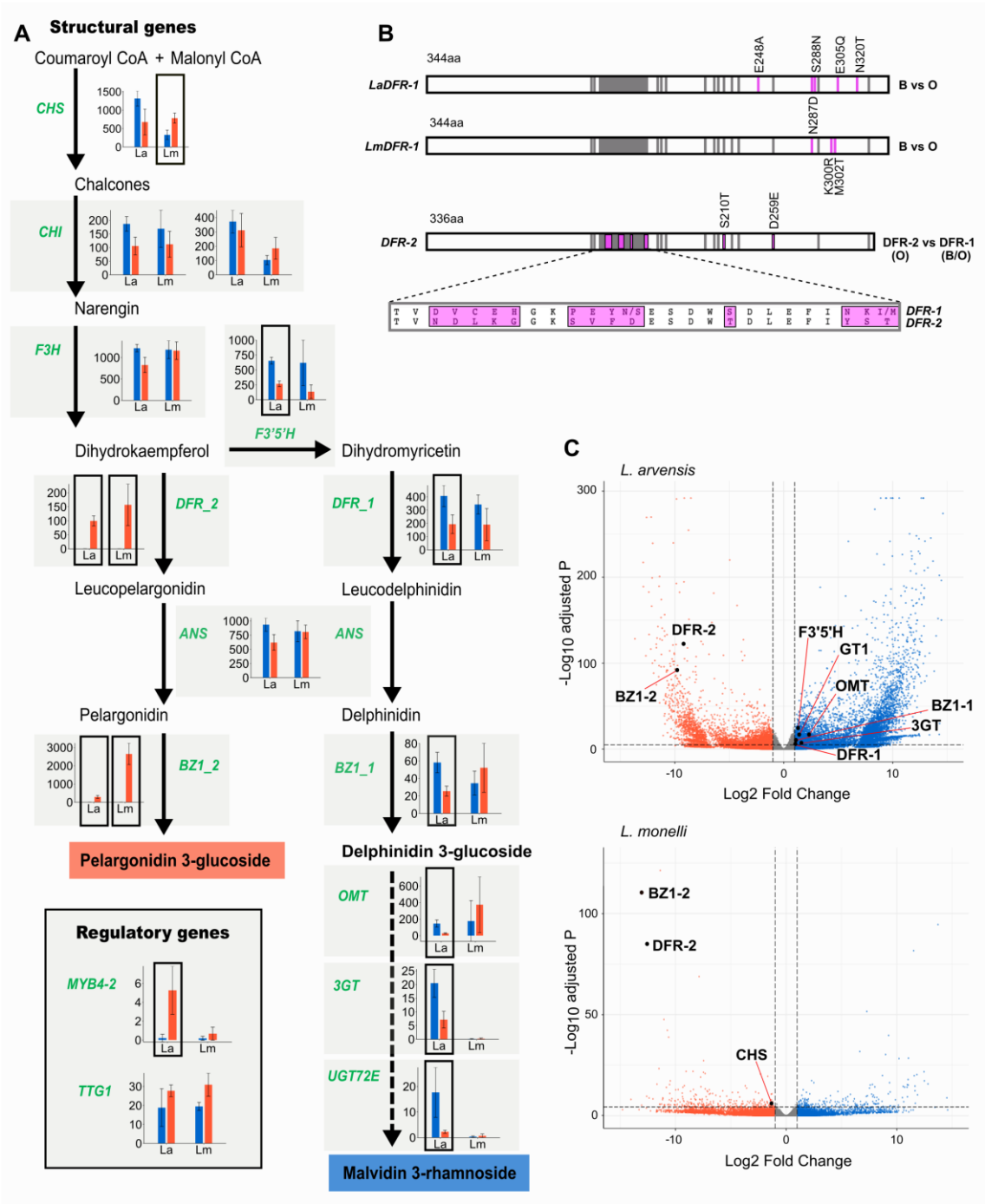

Figure 3. Gene expression comparisons of blue and orange morphs of two species of *Lysimachia*. (A) Suggested Anthocyanin Biosynthetic Pathway (ABP) producing blue (malvidin 3-rhamnoside) and orange (pelargonidin 3-glucoside) flower colors in these two species. Mean expression (TMM +/- standard error) in both species (La and Lm) are shown for each ABP gene (green font). Significantly differentially expressed genes (DEGs) are indicated with a black box around the bar plots. (B) Diagrams of the *DFR* coding sequence showing color-differentiating non-synonymous SNPs in pink (>70% frequency difference) between blue and orange *DFR-1* of *L. arvensis* and *L. monelli*,

and differences between *DFR-1* (blue and orange) and *DFR-2* (orange) of both species. Gray areas indicate substrate specificity and active sites of *DFR* genes. The magnified region comparing *DFR-1* and *DFR-2* shows many NS SNPs (pink) in the largest substrate specificity region. (C) Volcano plot comparing the entire transcriptomes of *L. arvensis* and *L. monelli* highlighting ABP genes with significant differential expression.

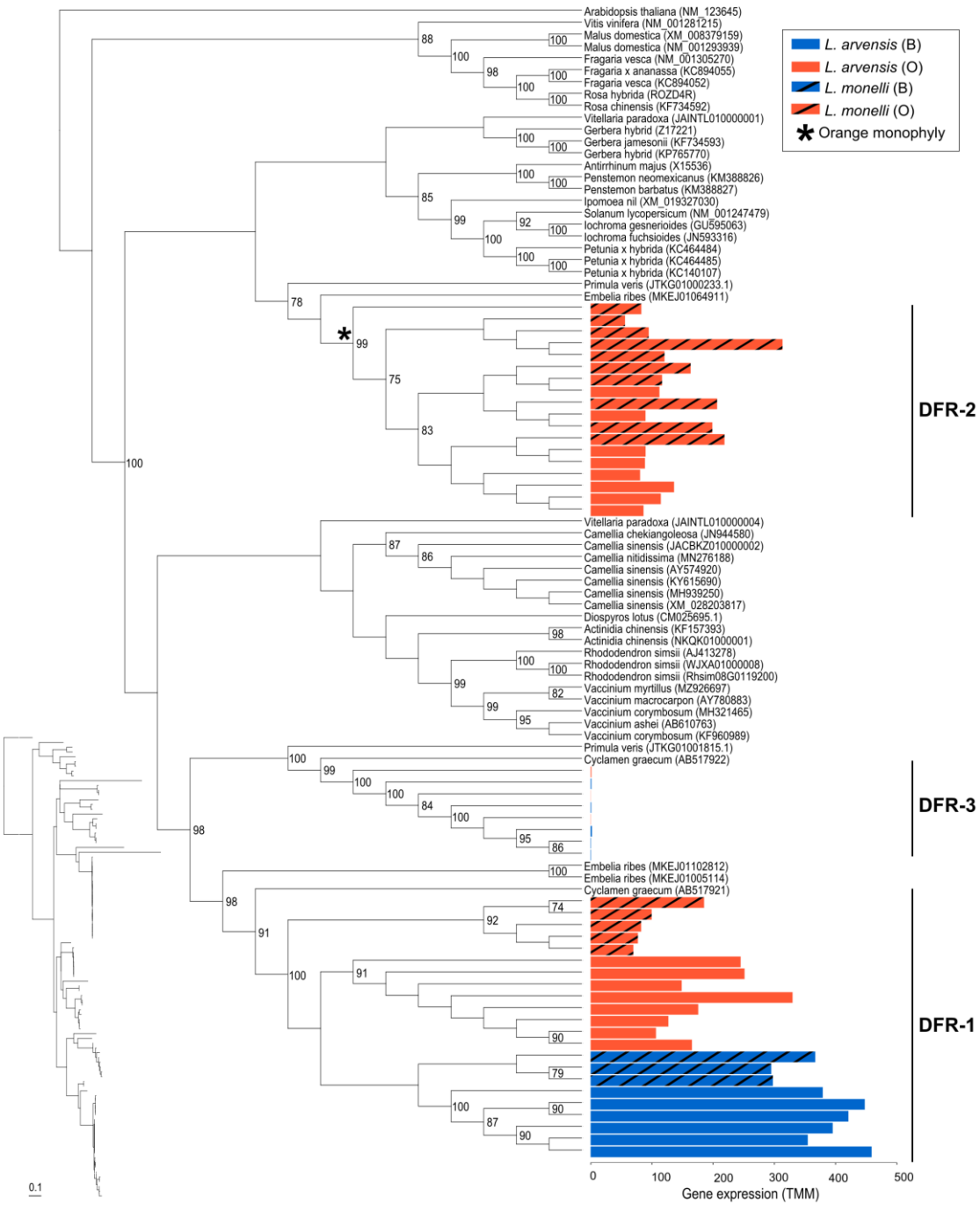

Figure 4. Maximum likelihood cladogram of the coding sequences of three *DFR* paralogues expressed in two *Lysimachia* species. Outgroups were selected from top BLASTn hits and, when available, from the genomes of closely related species (*Camelia sinensis*, *Embelia ribes* and *Primula veris*). Outgroups are indicated by scientific name followed by Genbank Accession numbers. Bootstrap values are provided to the right of the nodes when greater than 70%. The bar plot shows the expression level (TMM) for blue and orange flowers of *L. arvensis* (solid) and *L.*

monelli (black stripes). The monophyletic clade of orange petal samples for *DFR-2* is indicated with an asterisk (*). A phylogram (inset) is provided with the samples in the same order as the cladogram to compare relative branch lengths. Scale bar is in substitutions per site.

887 **Table 1.** Evidence for a single origin versus convergent evolution of the blue to orange flower color shift in *Lm* and *La*.

Evidence	Evidence for trans-specific polymorphism	Evidence for convergent evolution
UV-vis spectra	7x more variation between color morphs than between species (Figure 1B; Appendix 1—figure 1)	In the UV, two peaks for *Lm*-O vs. one peak + a shoulder for *La*-O and in the visible wavelengths there are some small differences in the inflection points (Figure 1B)
Biochemistry	Identical anthocyanins detected in both species and no significant differences in the relative concentrations for each color morph between species (Figure 1C)	None
Expression – structural genes	Significant upregulation of *DFR-2* and *BZ1-2* in orange morphs of both species (Figure 3A)	Compensatory downregulation of the *F3'5'H*, *DFR-1* and *BZ1-1* in orange morphs is only significant in *La* (but *F3'5'H* and *DFR-1* trend toward downregulation in orange *Lm*) (Figure 3A); *CHS*, *OMT*, *3GT* and *UGT72E* are DEGs in *La*, but not *Lm* (Figure 3A)
Expression – regulatory genes	*MYB4-2* (negative regulator of ABP structural genes) has higher expression in orange morphs of both species (but is only significant in *La*; Figure 3A)	No single known ABP regulatory locus with significant expression differences between blue and orange morphs for both species.

Expression correlations	*DFR-2* and *BZ1-2* are strongly correlated with each other in both species and *BZ1-2* is significantly correlated with the positive regulator *TTG1* in both species; *DFR-1* is negatively correlated with *MYB4-2* in orange morphs of both species (Appendix 1—figure 4)	Correlation between *DFR-2* and *TTG1* is only significantly in *La* after Bonferroni correction (but they have a strong positive association in *Lm*)
SNPs – structural genes	*DFR-2* of orange morphs of both species have the same 13 NS SNPs which overlap with a known pelargonidin-specific domain (Figure 3B)	*bHLH12* exhibits reciprocal monophyly of species (Appendix 1—figure 2J), however no NS SNPs differentiate color morphs in either species
SNPs – regulatory genes	*MYB4-2* has two NS SNPs in both species	*MYB4-2*'s NS SNPs do not overlap with known functional domains; *F3'H* has five NS SNPs in *Lm*-orange and only one in *La*-orange
Climate niche modeling	Three temperature-related variables have parallel effects on color morphs for both species (orange = cooler than blue; Appendix 1—table 4A)	Six variables (mostly precipitation-related) have opposing effects on color morphs in the two species (orange *Lm* = dry vs. orange *La* = wet; Appendix 1—table 4A).

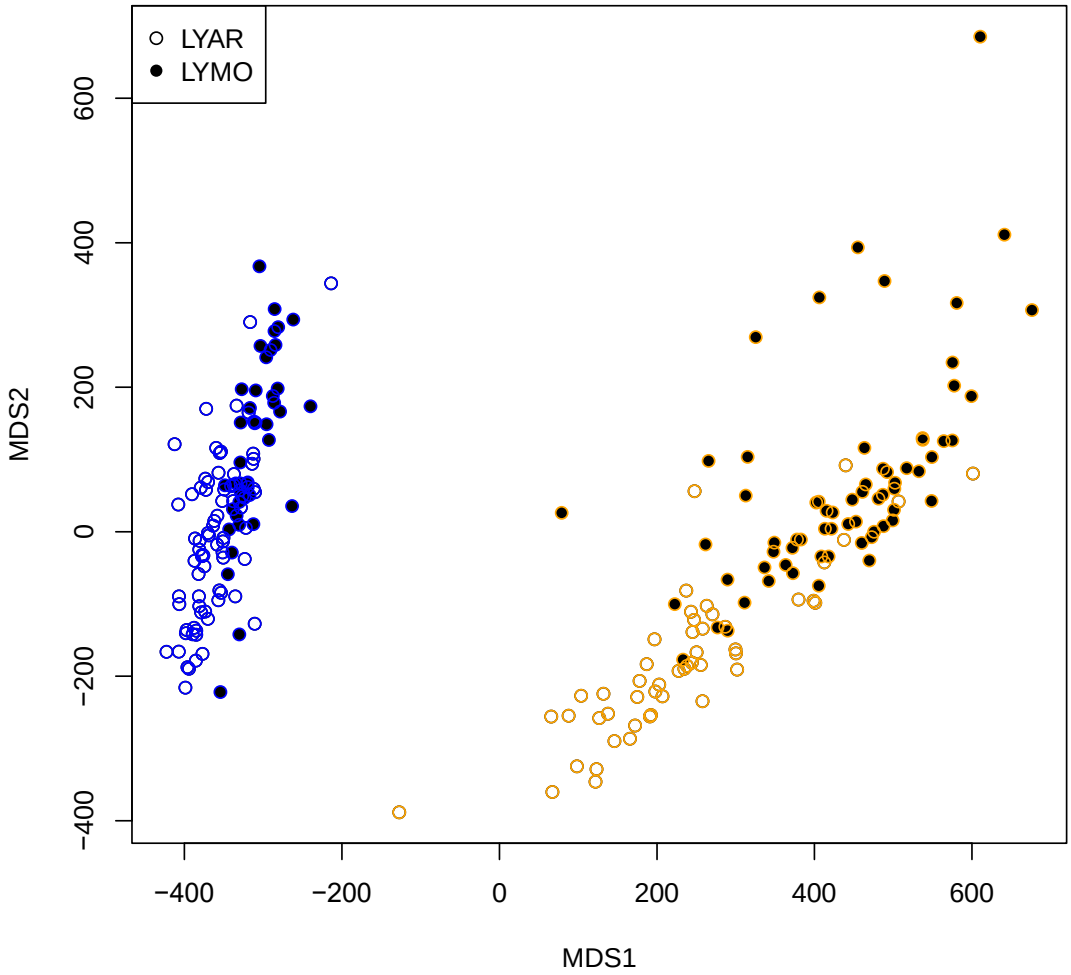

Appendix 1—figure 1. NMDS plot of UV-Vis reflectance spectra for blue and orange petalled individuals of *L. arvensis* (LYAR) and *L. monelli*. Statistical analysis was assessed with permutational manova (Anderson, 2001) with the following results (1) restricting permutations within color (comparing across species), $R^2 = 0.15113$, $F = 41.662$, $p < 1e\text{-}04$ vs. (2) restricting permutations within species (comparing across colors), $R^2 = 0.74999$, $F = 701.98$, $p < 1e\text{-}04$. Very similar results were found after applying a brightness correction – subtracting the minimum reflectance value of each sample from all wavelengths (not shown).

BZ1-2 and -3

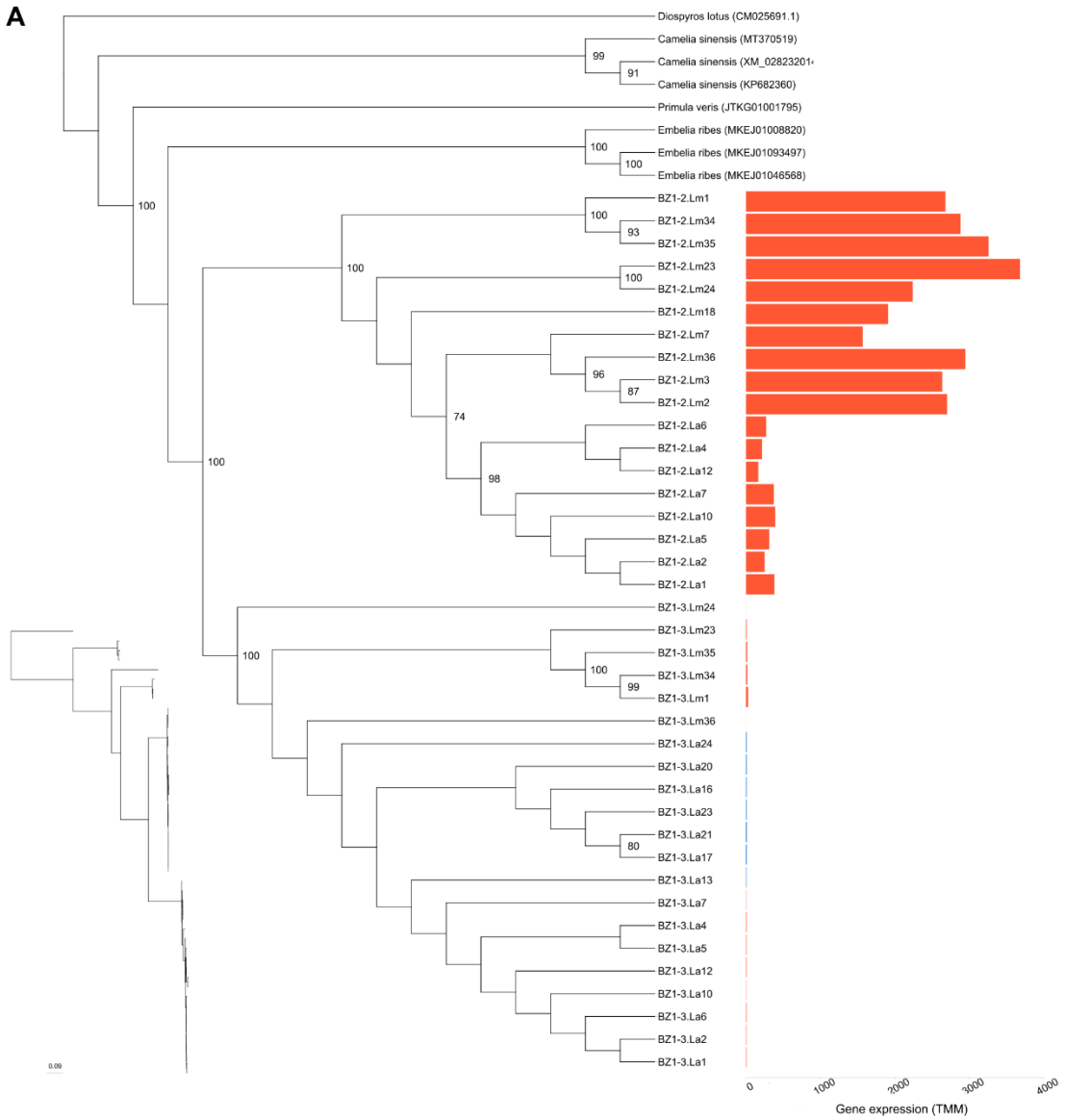
A
Diospyros lotus (CM025691.1)
Camelia sinensis (MT370519)
Camelia sinensis (XM_02823201
Camelia sinensis (KP682360)
Primula veris (JTKG01001795)
Embelia ribes (MKEJ01008820)
Embelia ribes (MKEJ01093497)
Embelia ribes (MKEJ01046568)
BZ1-2.Lm1
BZ1-2.Lm34
BZ1-2.Lm35
BZ1-2.Lm23
BZ1-2.Lm24
BZ1-2.Lm18
BZ1-2.Lm7
BZ1-2.Lm36
BZ1-2.Lm3
BZ1-2.Lm2
BZ1-2.La6
BZ1-2.La4
BZ1-2.La12
BZ1-2.La7
BZ1-2.La10
BZ1-2.La5
BZ1-2.La2
BZ1-2.La1
BZ1-3.Lm24
BZ1-3.Lm23
BZ1-3.Lm35
BZ1-3.Lm34
BZ1-3.Lm1
BZ1-3.Lm36
BZ1-3.La24
BZ1-3.La20
BZ1-3.La16
BZ1-3.La23
BZ1-3.La21
BZ1-3.La17
BZ1-3.La13
BZ1-3.La7
BZ1-3.La4
BZ1-3.La5
BZ1-3.La12
BZ1-3.La10
BZ1-3.La6
BZ1-3.La2
BZ1-3.La1
0.09
0
1000
2000
3000
4000
Gene expression (TMM)

Caffeoyl CoA-1,-2 and *-3*.

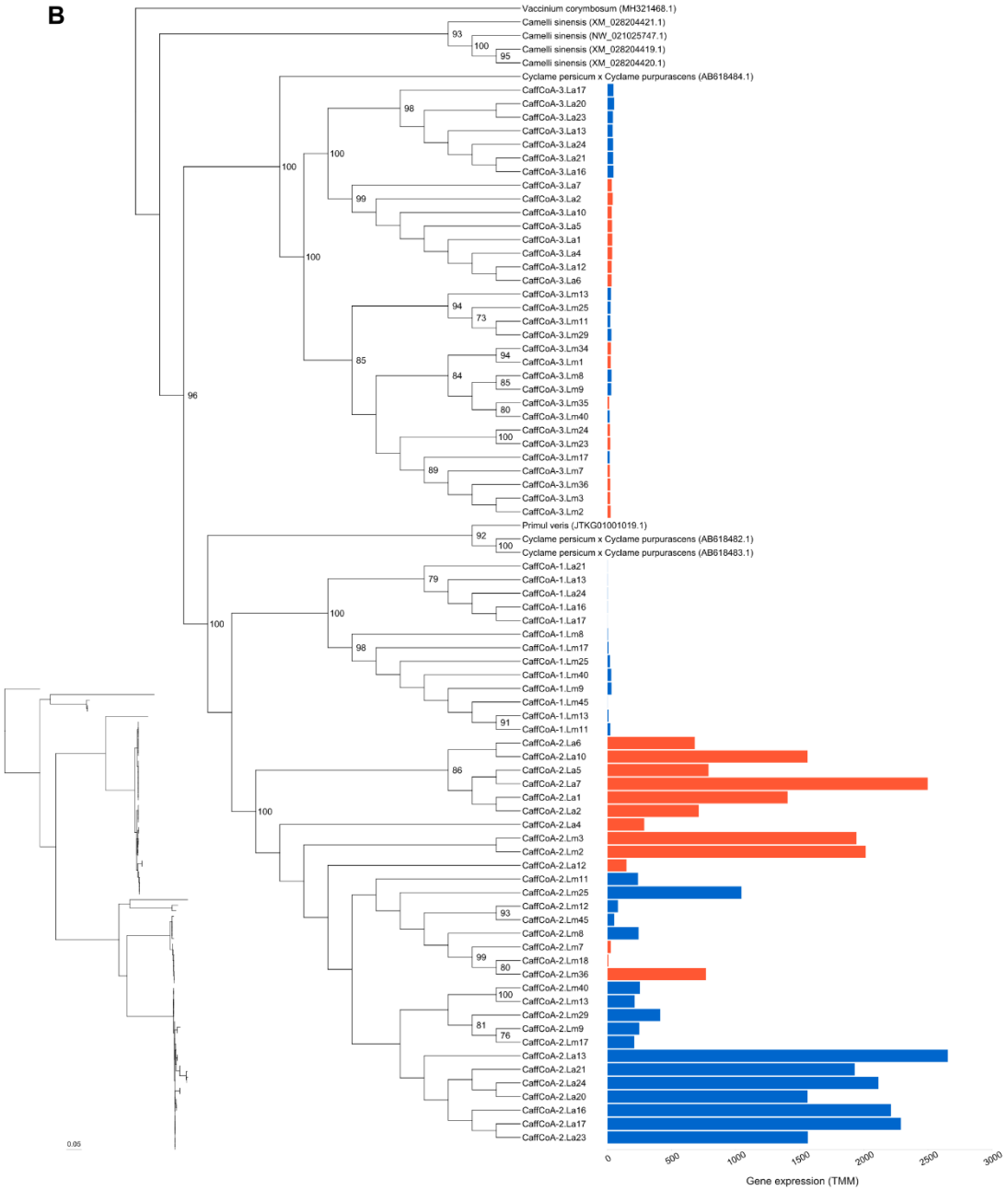

CHS

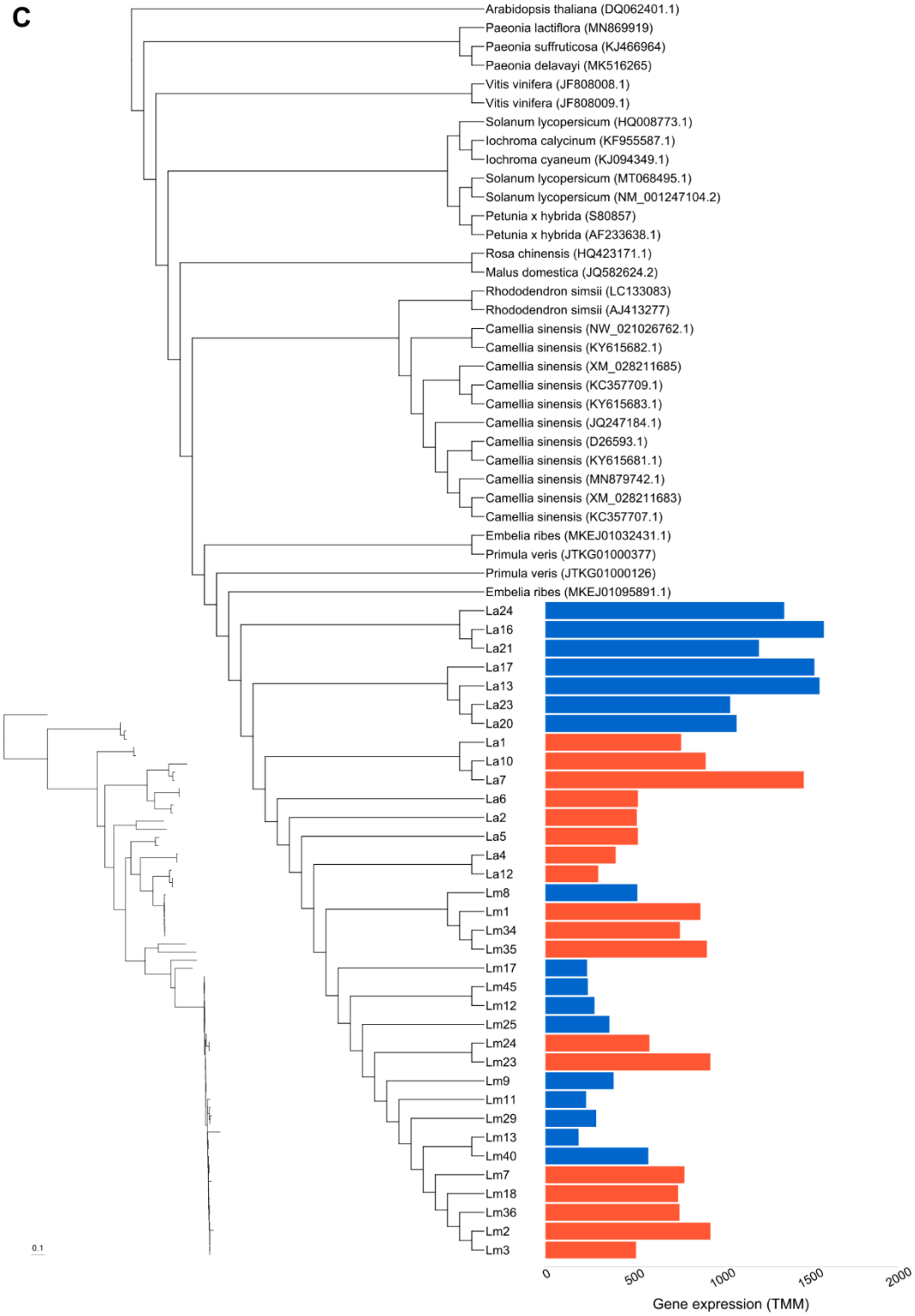
C
Arabidopsis thaliana (DQ062401.1)
Paeonia lactiflora (MN869919)
Paeonia suffruticosa (KJ466964)
Paeonia delavayi (MK516265)
Vitis vinifera (JF808008.1)
Vitis vinifera (JF808009.1)
Solanum lycopersicum (HQ008773.1)
Iochroma calycinum (KF955587.1)
Iochroma cyaneum (KJ094349.1)
Solanum lycopersicum (MT068495.1)
Solanum lycopersicum (NM_001247104.2)
Petunia x hybrida (S80857)
Petunia x hybrida (AF233638.1)
Rosa chinensis (HQ423171.1)
Malus domestica (JQ582624.2)
Rhododendron simsii (LC133083)
Rhododendron simsii (AJ413277)
Camellia sinensis (NW_021026762.1)
Camellia sinensis (KY615682.1)
Camellia sinensis (XM_028211685)
Camellia sinensis (KC357709.1)
Camellia sinensis (KY615683.1)
Camellia sinensis (JQ247184.1)
Camellia sinensis (D26593.1)
Camellia sinensis (KY615681.1)
Camellia sinensis (MN879742.1)
Camellia sinensis (XM_028211683)
Camellia sinensis (KC357707.1)
Embelia ribes (MKEJ01032431.1)
Primula veris (JTKG01000377)
Primula veris (JTKG01000126)
Embelia ribes (MKEJ01095891.1)
La24
La16
La21
La17
La13
La23
La20
La1
La10
La7
La6
La2
La5
La4
La12
Lm8
Lm1
Lm34
Lm35
Lm17
Lm45
Lm12
Lm25
Lm24
Lm23
Lm9
Lm11
Lm29
Lm13
Lm40
Lm7
Lm18
Lm36
Lm2
Lm3
0.1
0
500
1000
1500
2000
Gene expression (TMM)

907 *F3'5'H*

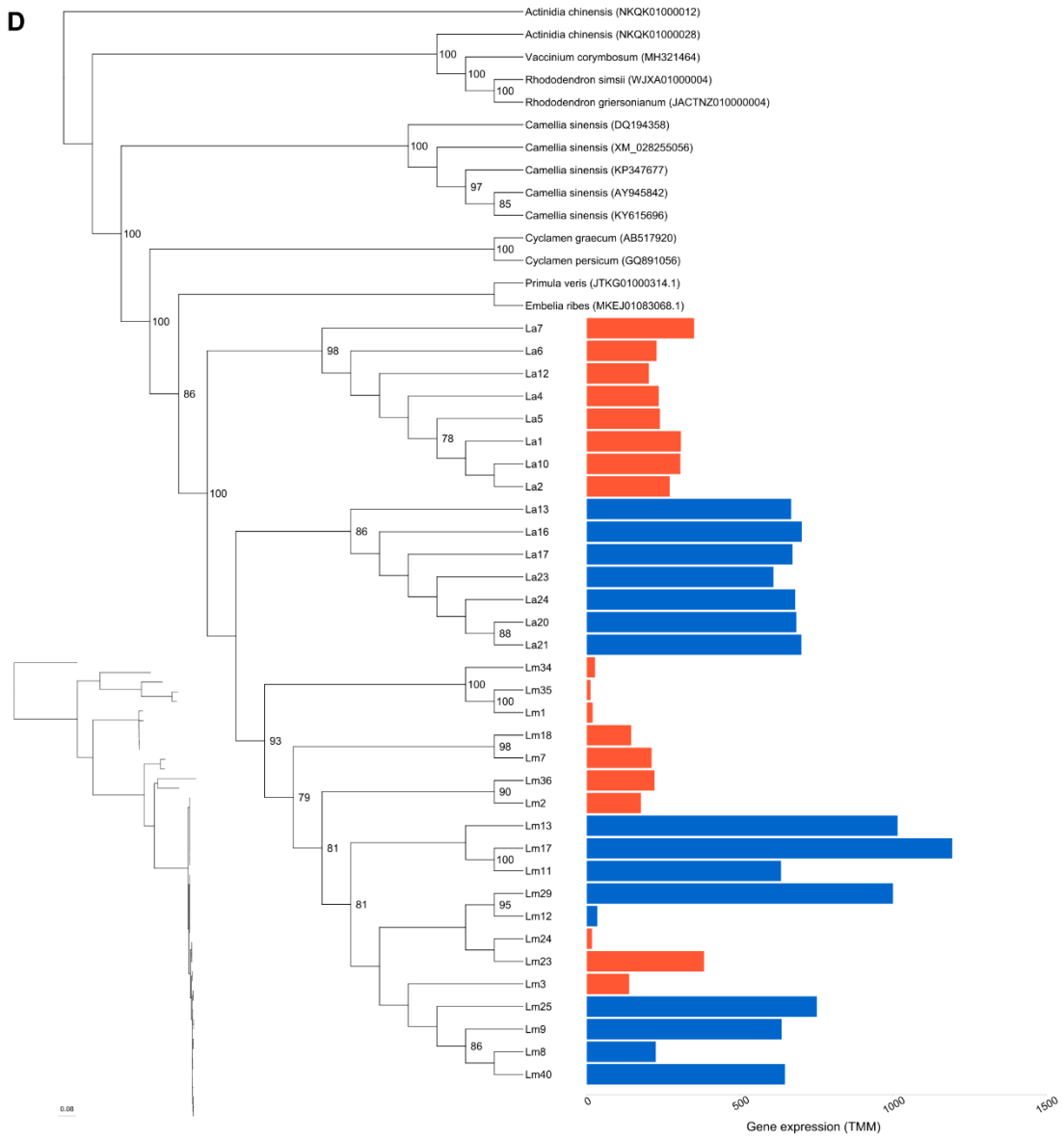

908

909

910 *F3'H*

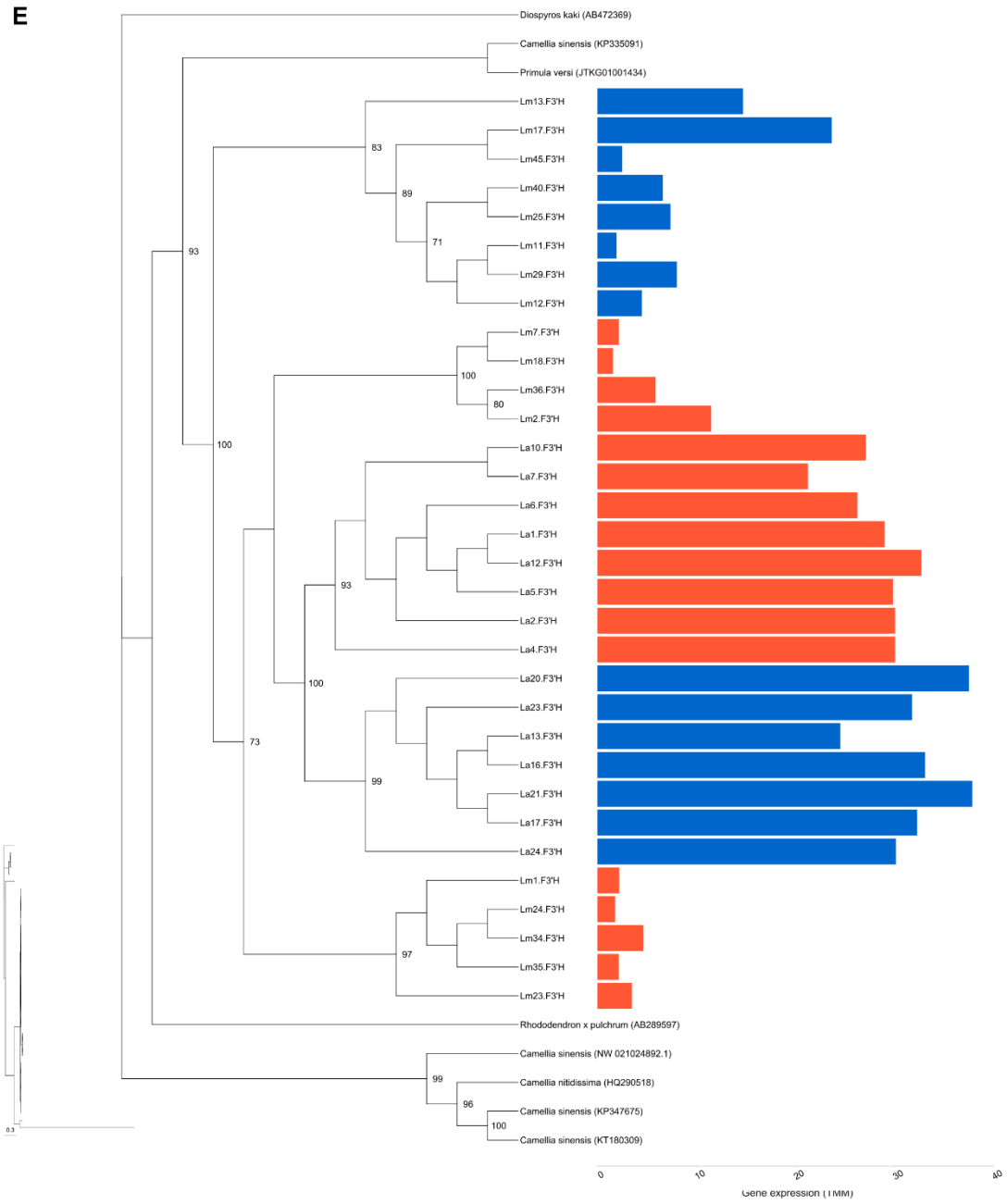
E
Diospyros kaki (AB472369)
Camellia sinensis (KP335091)
Primula versi (JTKG01001434)
Lm13.F3'H
Lm17.F3'H
Lm45.F3'H
Lm40.F3'H
Lm25.F3'H
Lm11.F3'H
Lm29.F3'H
Lm12.F3'H
Lm7.F3'H
Lm18.F3'H
Lm36.F3'H
Lm2.F3'H
La10.F3'H
La7.F3'H
La6.F3'H
La1.F3'H
La12.F3'H
La5.F3'H
La2.F3'H
La4.F3'H
La20.F3'H
La23.F3'H
La13.F3'H
La16.F3'H
La21.F3'H
La17.F3'H
La24.F3'H
Lm1.F3'H
Lm24.F3'H
Lm34.F3'H
Lm35.F3'H
Lm23.F3'H
Rhododendron x pulchrum (AB289597)
Camellia sinensis (NW 021024892.1)
Camellia nitidissima (HQ290518)
Camellia sinensis (KP347675)
Camellia sinensis (KT180309)
83
89
71
93
100
100
80
93
100
73
99
97
99
96
100
0
10
20
30
40
Gene expression (TMM)

911

AN11a

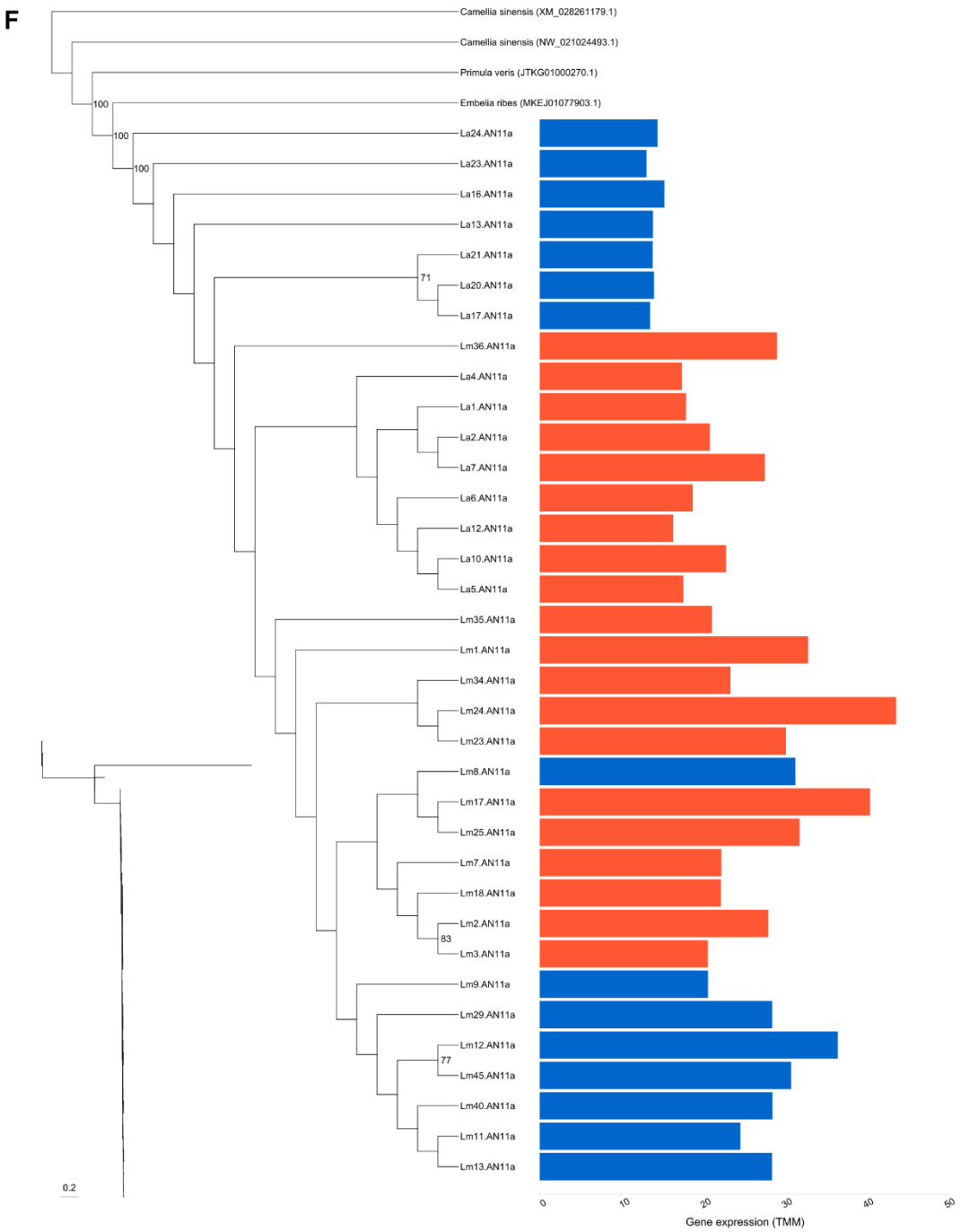
F
Camellia sinensis (XM_028261179.1)
Camellia sinensis (NW_021024493.1)
Primula veris (JTKG01000270.1)
Embelia ribes (MKEJ01077903.1)
La24.AN11a
La23.AN11a
La16.AN11a
La13.AN11a
La21.AN11a
La20.AN11a
La17.AN11a
Lm36.AN11a
La4.AN11a
La1.AN11a
La2.AN11a
La7.AN11a
La6.AN11a
La12.AN11a
La10.AN11a
La5.AN11a
Lm35.AN11a
Lm1.AN11a
Lm34.AN11a
Lm24.AN11a
Lm23.AN11a
Lm8.AN11a
Lm17.AN11a
Lm25.AN11a
Lm7.AN11a
Lm18.AN11a
Lm2.AN11a
Lm3.AN11a
Lm9.AN11a
Lm29.AN11a
Lm12.AN11a
Lm45.AN11a
Lm40.AN11a
Lm11.AN11a
Lm13.AN11a
100
100
100
71
83
77
0.2
0
10
20
30
40
50
Gene expression (TMM)

bHLH1

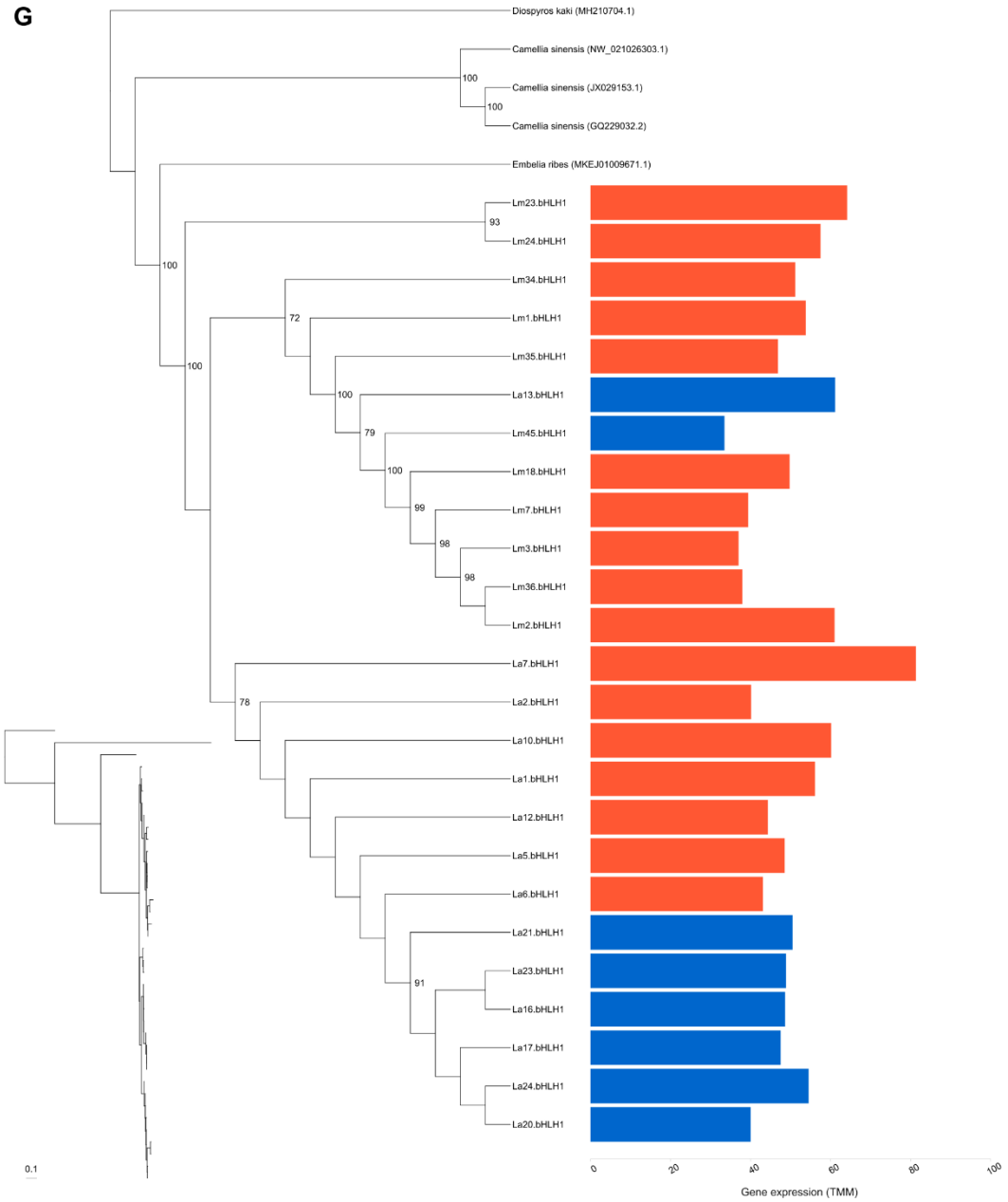
G
Diospyros kaki (MH210704.1)
Camellia sinensis (NW_021026303.1)
Camellia sinensis (JX029153.1)
Camellia sinensis (GQ229032.2)
Embelia ribes (MKEJ01009671.1)
Lm23.bHLH1
Lm24.bHLH1
Lm34.bHLH1
Lm1.bHLH1
Lm35.bHLH1
La13.bHLH1
Lm45.bHLH1
Lm18.bHLH1
Lm7.bHLH1
Lm3.bHLH1
Lm36.bHLH1
Lm2.bHLH1
La7.bHLH1
La2.bHLH1
La10.bHLH1
La1.bHLH1
La12.bHLH1
La5.bHLH1
La6.bHLH1
La21.bHLH1
La23.bHLH1
La16.bHLH1
La17.bHLH1
La24.bHLH1
La20.bHLH1
100
100
93
100
72
100
100
79
100
99
98
98
78
91
0.1
0
20
40
60
80
100
Gene expression (TMM)

bHLH2-2

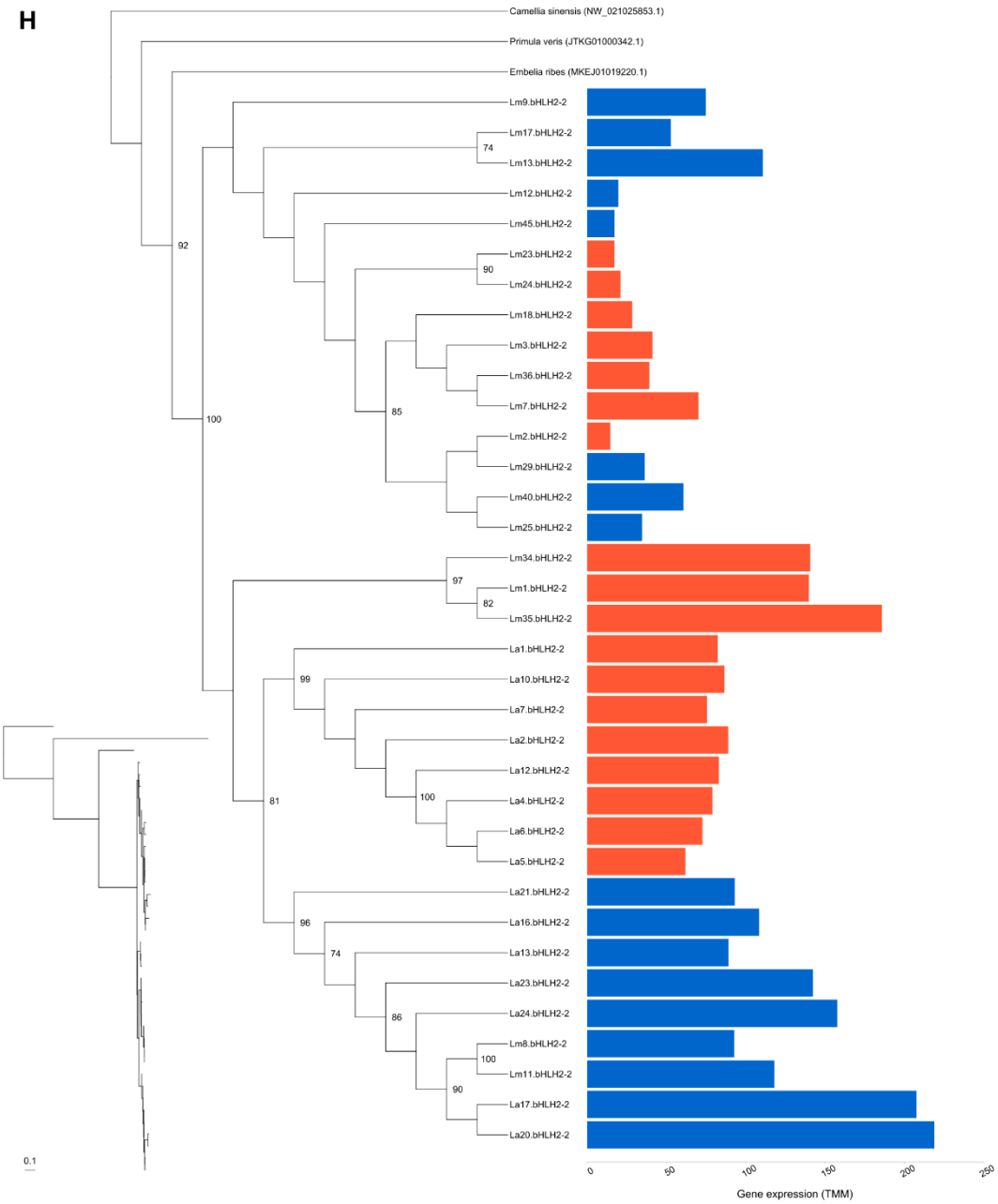
H
Camellia sinensis (NW_021025853.1)
Primula veris (JTKG01000342.1)
Embelia ribes (MKEJ01019220.1)
Lm9.bHLH2-2
Lm17.bHLH2-2
Lm13.bHLH2-2
Lm12.bHLH2-2
Lm45.bHLH2-2
Lm23.bHLH2-2
Lm24.bHLH2-2
Lm18.bHLH2-2
Lm3.bHLH2-2
Lm36.bHLH2-2
Lm7.bHLH2-2
Lm2.bHLH2-2
Lm29.bHLH2-2
Lm40.bHLH2-2
Lm25.bHLH2-2
Lm34.bHLH2-2
Lm1.bHLH2-2
Lm35.bHLH2-2
La1.bHLH2-2
La10.bHLH2-2
La7.bHLH2-2
La2.bHLH2-2
La12.bHLH2-2
La4.bHLH2-2
La6.bHLH2-2
La5.bHLH2-2
La21.bHLH2-2
La16.bHLH2-2
La13.bHLH2-2
La23.bHLH2-2
La24.bHLH2-2
Lm8.bHLH2-2
Lm11.bHLH2-2
La17.bHLH2-2
La20.bHLH2-2
74
92
90
100
85
97
82
99
100
81
96
74
86
100
90
0.1
0
50
100
150
200
250
Gene expression (TMM)

bHLH2-3

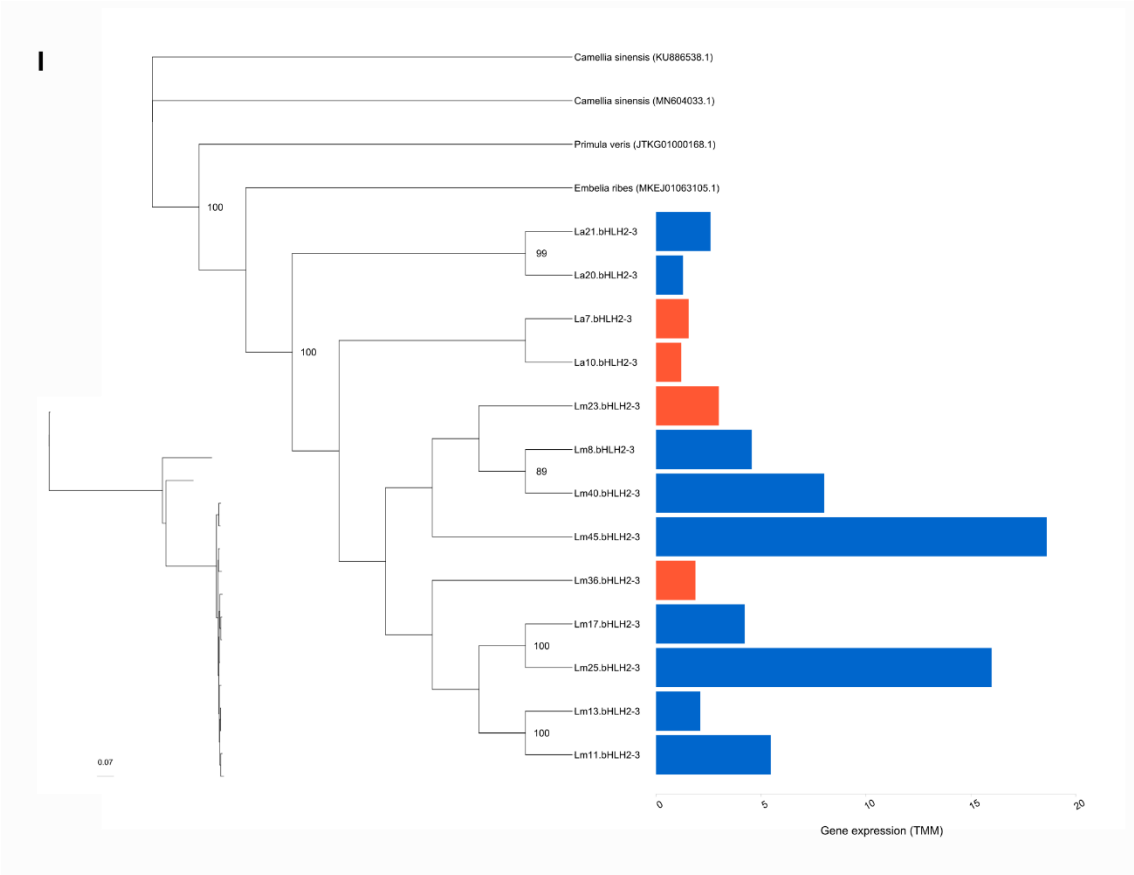
I
Camellia sinensis (KU886538.1)
Camellia sinensis (MN604033.1)
Primula veris (JTKG01000168.1)
Embelia ribes (MKEJ01063105.1)
100
La21.bHLH2-3
99
La20.bHLH2-3
La7.bHLH2-3
100
La10.bHLH2-3
Lm23.bHLH2-3
Lm8.bHLH2-3
89
Lm40.bHLH2-3
Lm45.bHLH2-3
Lm36.bHLH2-3
Lm17.bHLH2-3
100
Lm25.bHLH2-3
Lm13.bHLH2-3
100
Lm11.bHLH2-3
0.07
0
5
10
15
20
Gene expression (TMM)

bHLH12

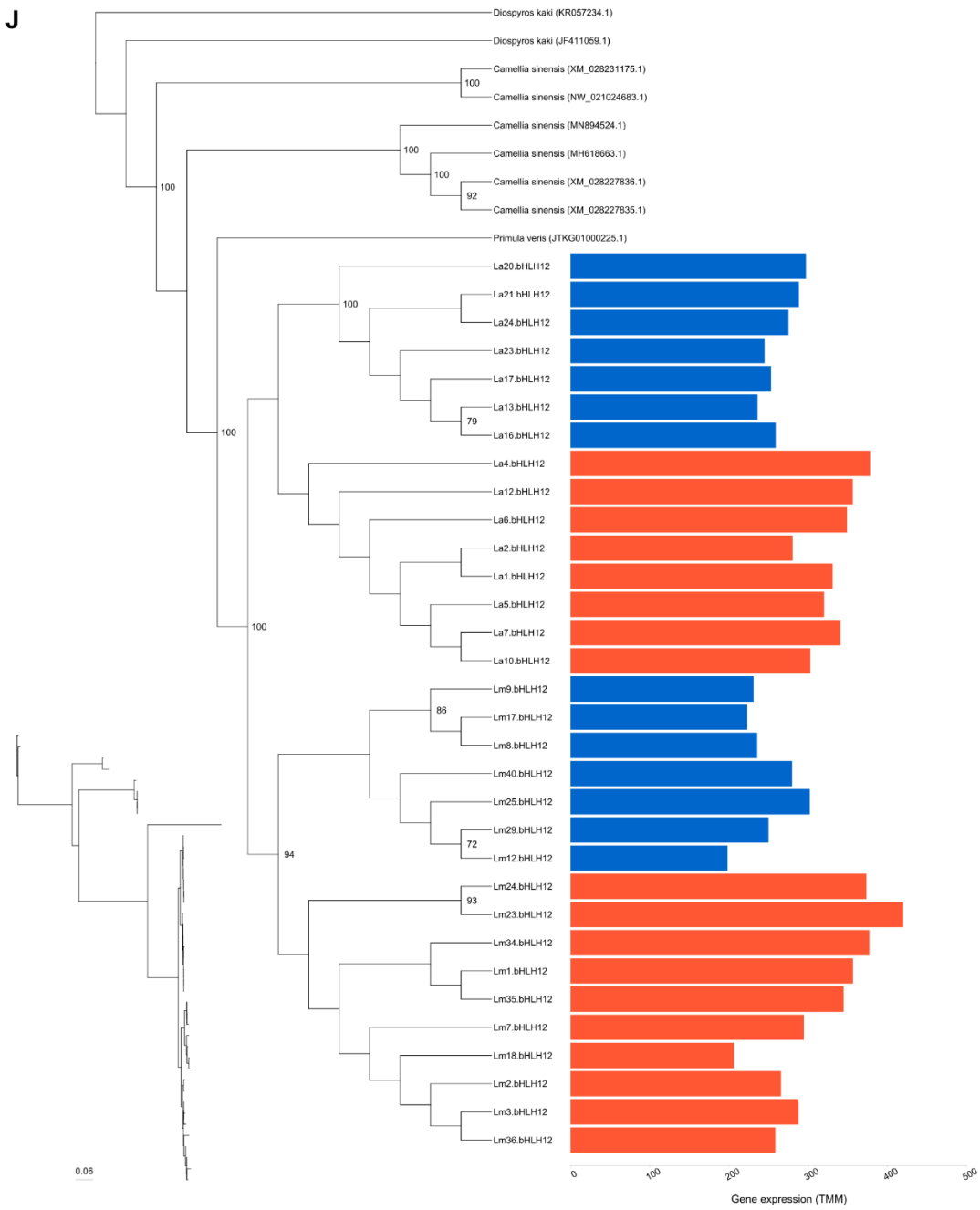
J
Diospyros kaki (KR057234.1)
Diospyros kaki (JF411059.1)
Camellia sinensis (XM_028231175.1)
Camellia sinensis (NW_021024683.1)
Camellia sinensis (MN894524.1)
Camellia sinensis (MH618663.1)
Camellia sinensis (XM_028227836.1)
Camellia sinensis (XM_028227835.1)
Primula veris (JTKG01000225.1)
La20.bHLH12
La21.bHLH12
La24.bHLH12
La23.bHLH12
La17.bHLH12
La13.bHLH12
La16.bHLH12
La4.bHLH12
La12.bHLH12
La6.bHLH12
La2.bHLH12
La1.bHLH12
La5.bHLH12
La7.bHLH12
La10.bHLH12
Lm9.bHLH12
Lm17.bHLH12
Lm8.bHLH12
Lm40.bHLH12
Lm25.bHLH12
Lm29.bHLH12
Lm12.bHLH12
Lm24.bHLH12
Lm23.bHLH12
Lm34.bHLH12
Lm1.bHLH12
Lm35.bHLH12
Lm7.bHLH12
Lm18.bHLH12
Lm2.bHLH12
Lm3.bHLH12
Lm36.bHLH12
100
100
100
100
92
100
100
79
100
86
94
72
93
0.06
0
100
200
300
400
500
Gene expression (TMM)

COP1

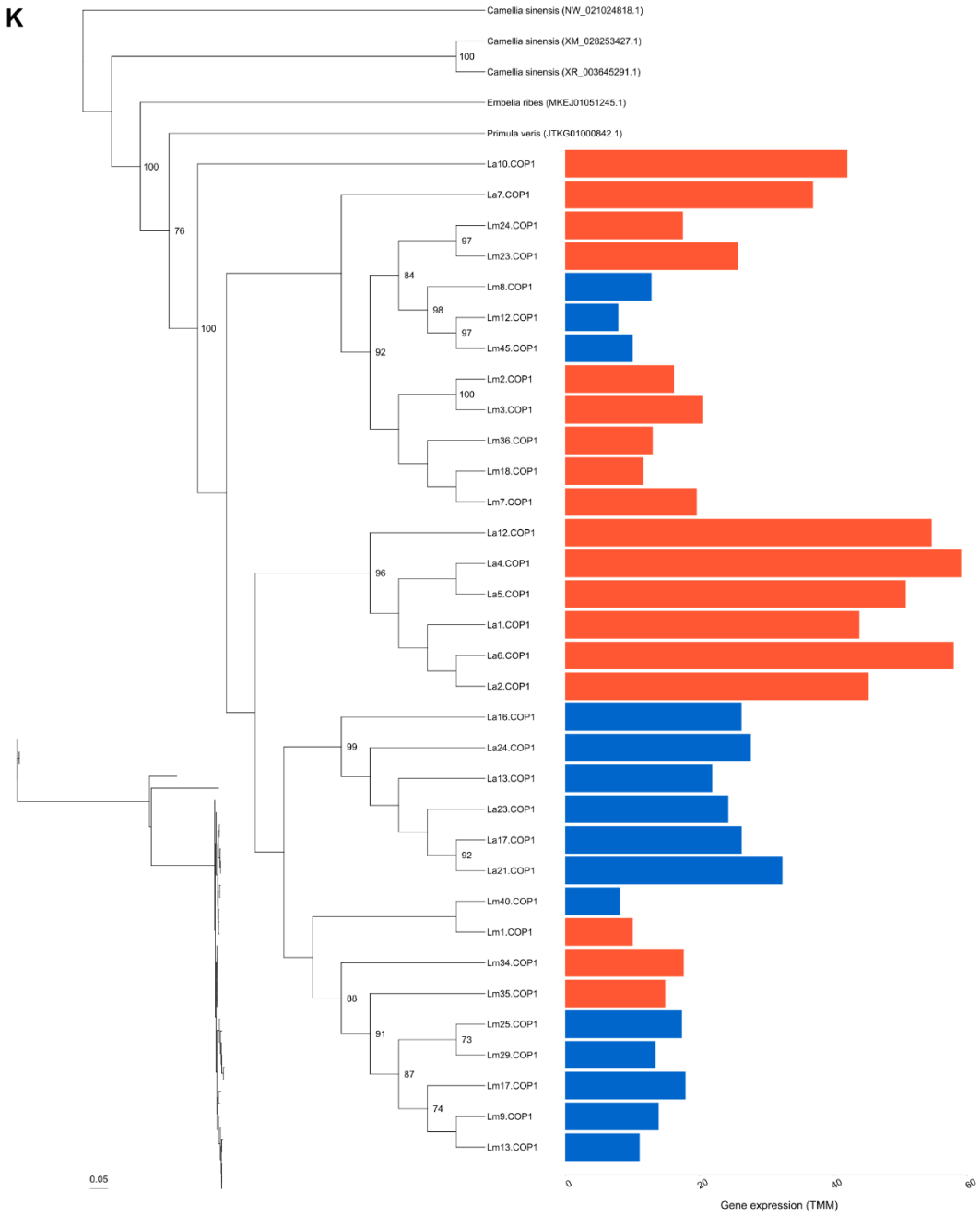
K
Camellia sinensis (NW_021024818.1)
Camellia sinensis (XM_028253427.1)
Camellia sinensis (XR_003645291.1)
Embelia ribes (MKEJ01051245.1)
Primula veris (JTKG01000842.1)
La10.COP1
La7.COP1
Lm24.COP1
Lm23.COP1
Lm8.COP1
Lm12.COP1
Lm45.COP1
Lm2.COP1
Lm3.COP1
Lm36.COP1
Lm18.COP1
Lm7.COP1
La12.COP1
La4.COP1
La5.COP1
La1.COP1
La6.COP1
La2.COP1
La16.COP1
La24.COP1
La13.COP1
La23.COP1
La17.COP1
La21.COP1
Lm40.COP1
Lm1.COP1
Lm34.COP1
Lm35.COP1
Lm25.COP1
Lm29.COP1
Lm17.COP1
Lm9.COP1
Lm13.COP1
100
76
100
97
84
98
97
92
100
96
99
92
88
91
73
87
74
0.05
0
20
40
60
Gene expression (TMM)

MYB4-1

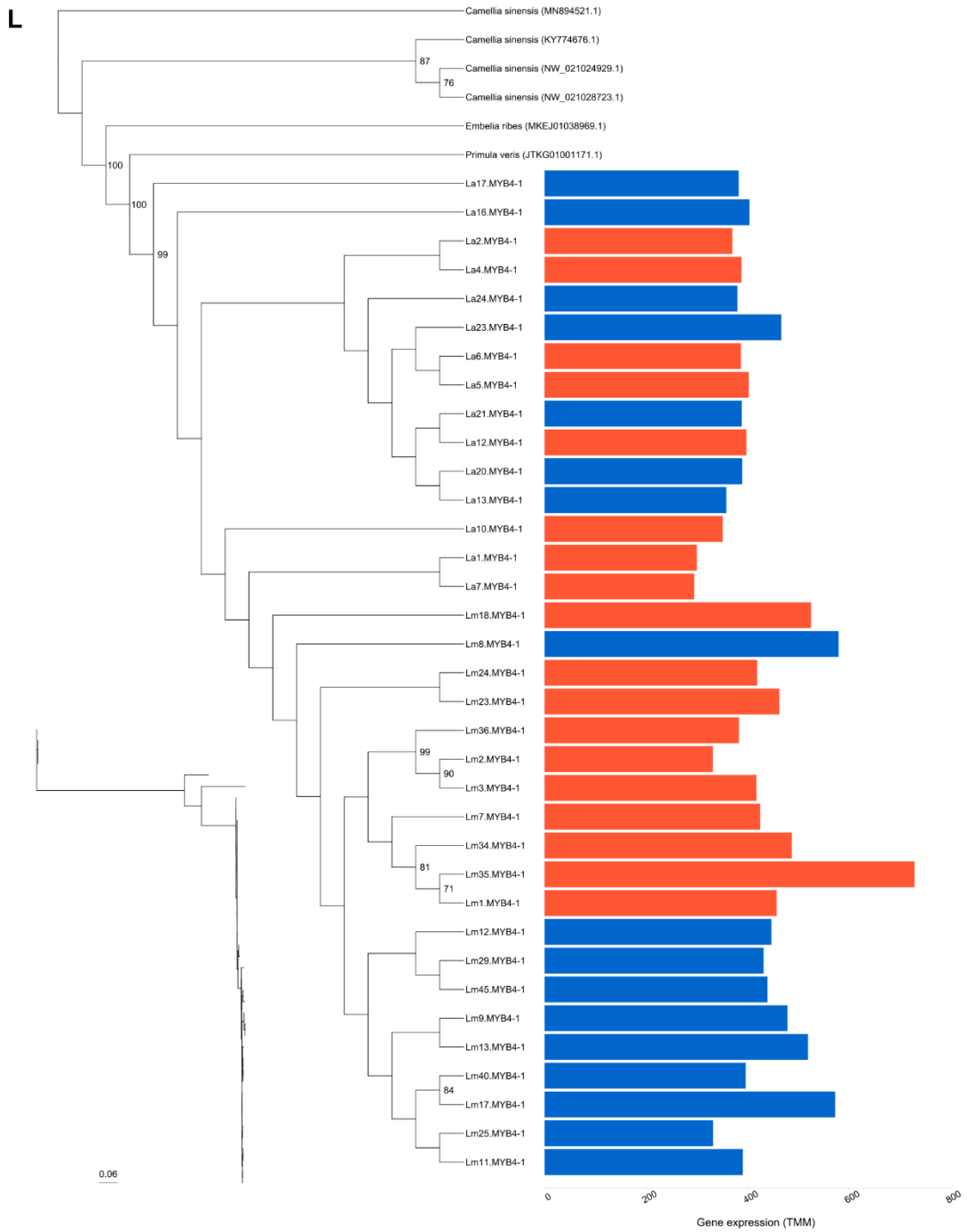
L
Camellia sinensis (MN894521.1)
Camellia sinensis (KY774676.1)
Camellia sinensis (NW_021024929.1)
Camellia sinensis (NW_021028723.1)
Embelia ribes (MKEJ01038969.1)
Primula veris (JTKG01001171.1)
La17.MYB4-1
La16.MYB4-1
La2.MYB4-1
La4.MYB4-1
La24.MYB4-1
La23.MYB4-1
La6.MYB4-1
La5.MYB4-1
La21.MYB4-1
La12.MYB4-1
La20.MYB4-1
La13.MYB4-1
La10.MYB4-1
La1.MYB4-1
La7.MYB4-1
Lm18.MYB4-1
Lm8.MYB4-1
Lm24.MYB4-1
Lm23.MYB4-1
Lm36.MYB4-1
Lm2.MYB4-1
Lm3.MYB4-1
Lm7.MYB4-1
Lm34.MYB4-1
Lm35.MYB4-1
Lm1.MYB4-1
Lm12.MYB4-1
Lm29.MYB4-1
Lm45.MYB4-1
Lm9.MYB4-1
Lm13.MYB4-1
Lm40.MYB4-1
Lm17.MYB4-1
Lm25.MYB4-1
Lm11.MYB4-1
87
76
100
100
99
99
90
81
71
84
0.06
0
200
400
600
800
Gene expression (TMM)

926 *MYB4-2*

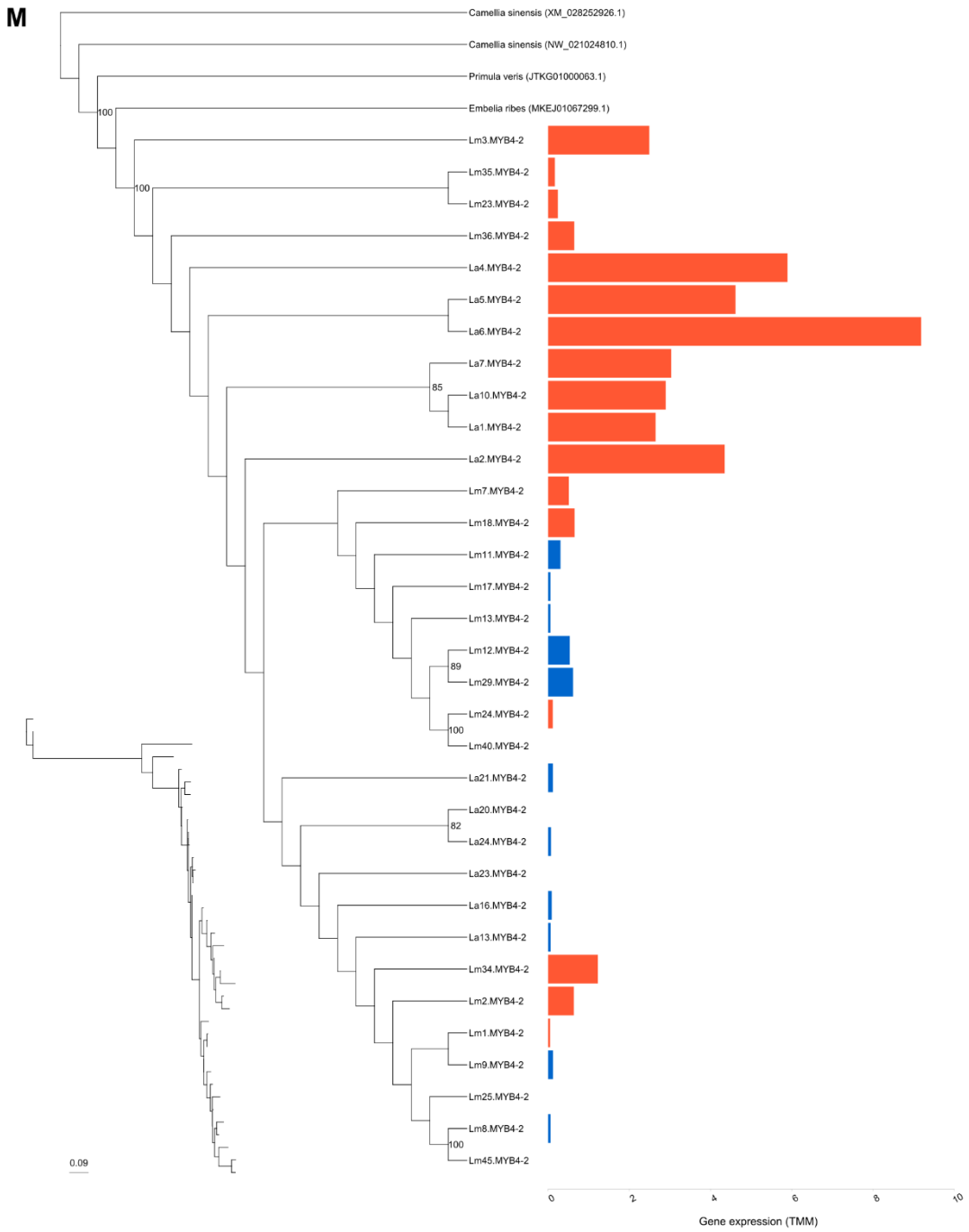

927

928 *MYB16-1*

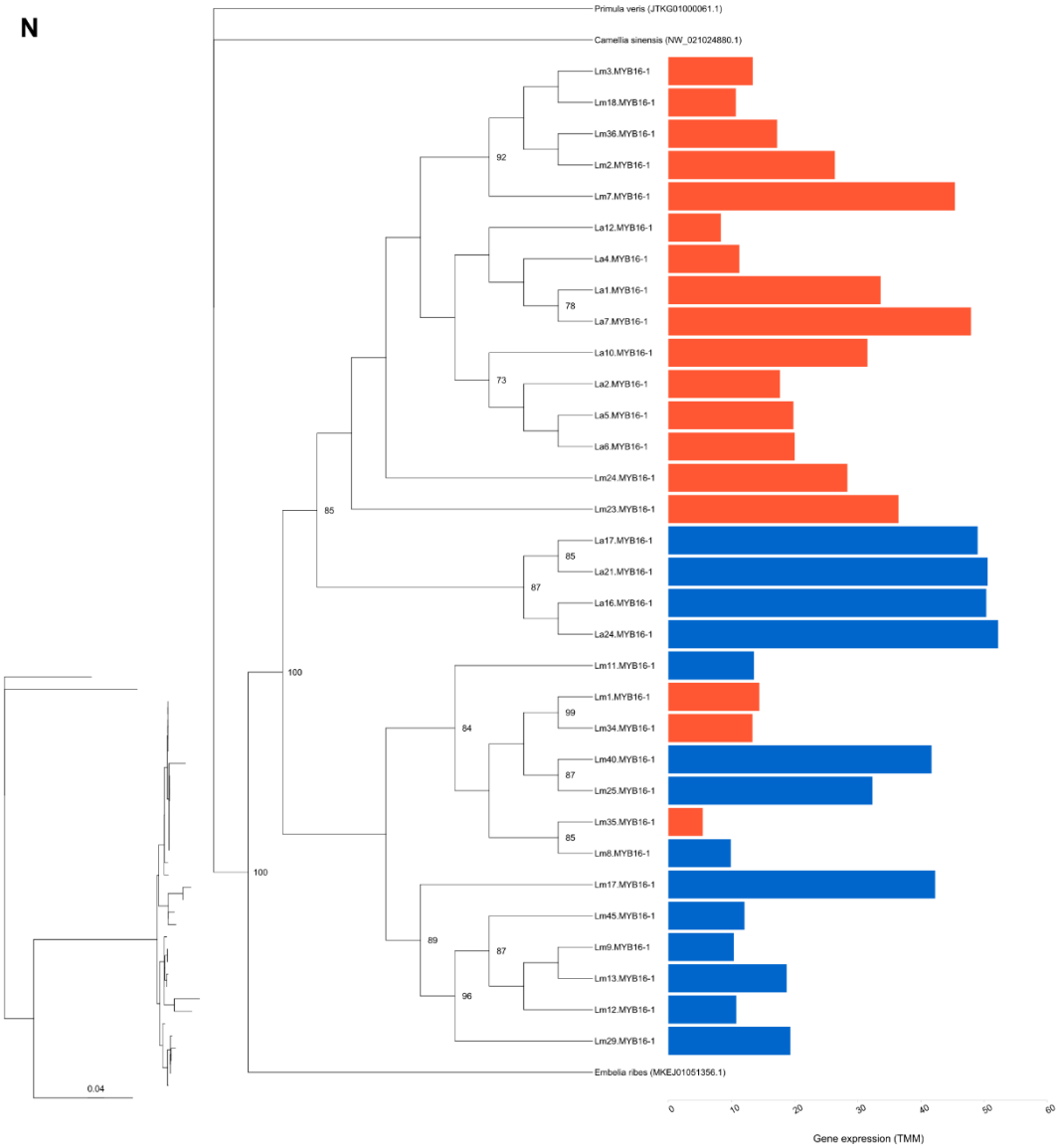

929

MYB16-2

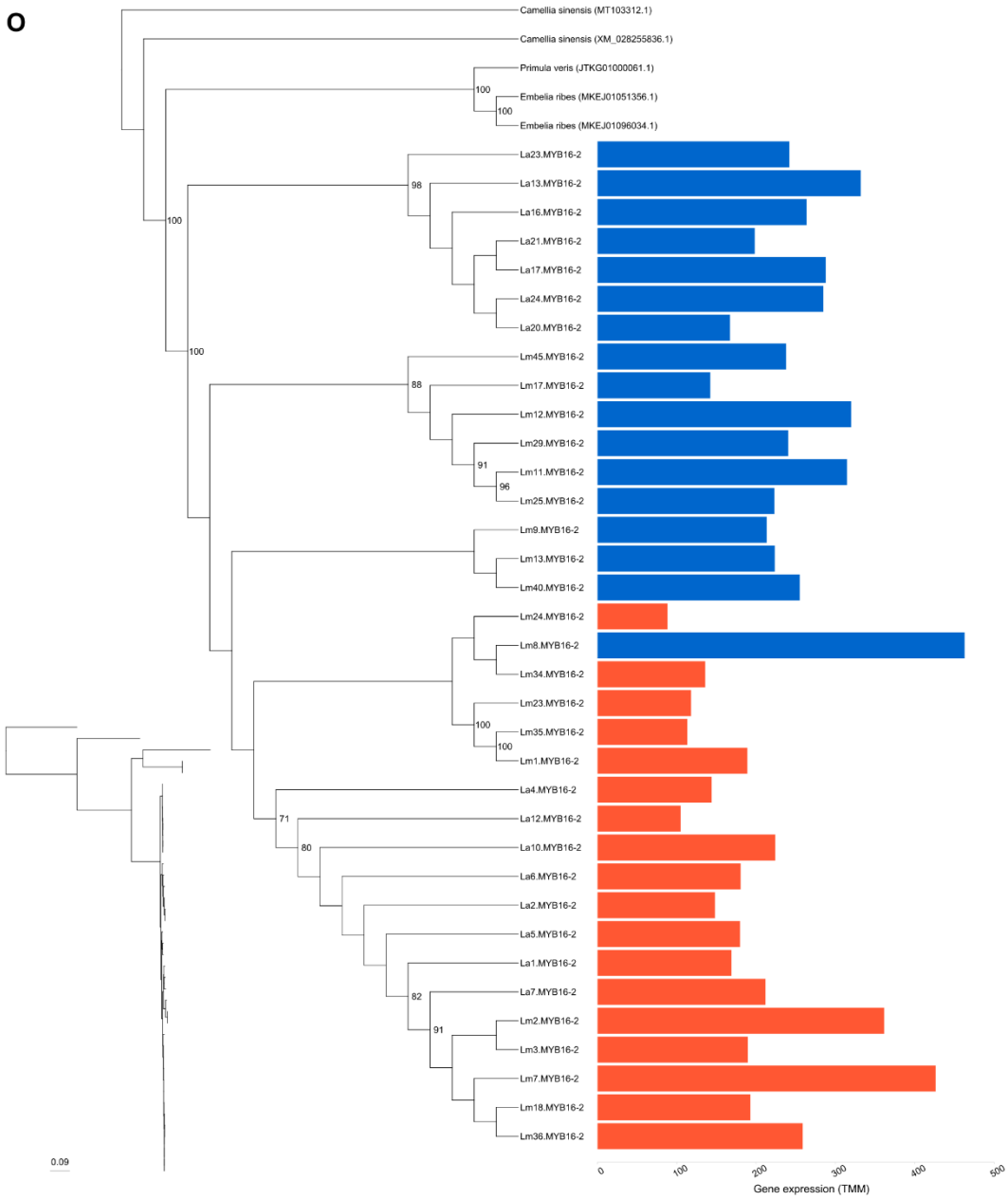
O
Camellia sinensis (MT103312.1)
Camellia sinensis (XM_028255836.1)
Primula veris (JTKG01000061.1)
Embelia ribes (MKEJ01051356.1)
Embelia ribes (MKEJ01096034.1)
La23.MYB16-2
La13.MYB16-2
La16.MYB16-2
La21.MYB16-2
La17.MYB16-2
La24.MYB16-2
La20.MYB16-2
Lm45.MYB16-2
Lm17.MYB16-2
Lm12.MYB16-2
Lm29.MYB16-2
Lm11.MYB16-2
Lm25.MYB16-2
Lm9.MYB16-2
Lm13.MYB16-2
Lm40.MYB16-2
Lm24.MYB16-2
Lm8.MYB16-2
Lm34.MYB16-2
Lm23.MYB16-2
Lm35.MYB16-2
Lm1.MYB16-2
La4.MYB16-2
La12.MYB16-2
La10.MYB16-2
La6.MYB16-2
La2.MYB16-2
La5.MYB16-2
La1.MYB16-2
La7.MYB16-2
Lm2.MYB16-2
Lm3.MYB16-2
Lm7.MYB16-2
Lm18.MYB16-2
Lm36.MYB16-2
0.09
0
100
200
300
400
500
Gene expression (TMM)

SPA1

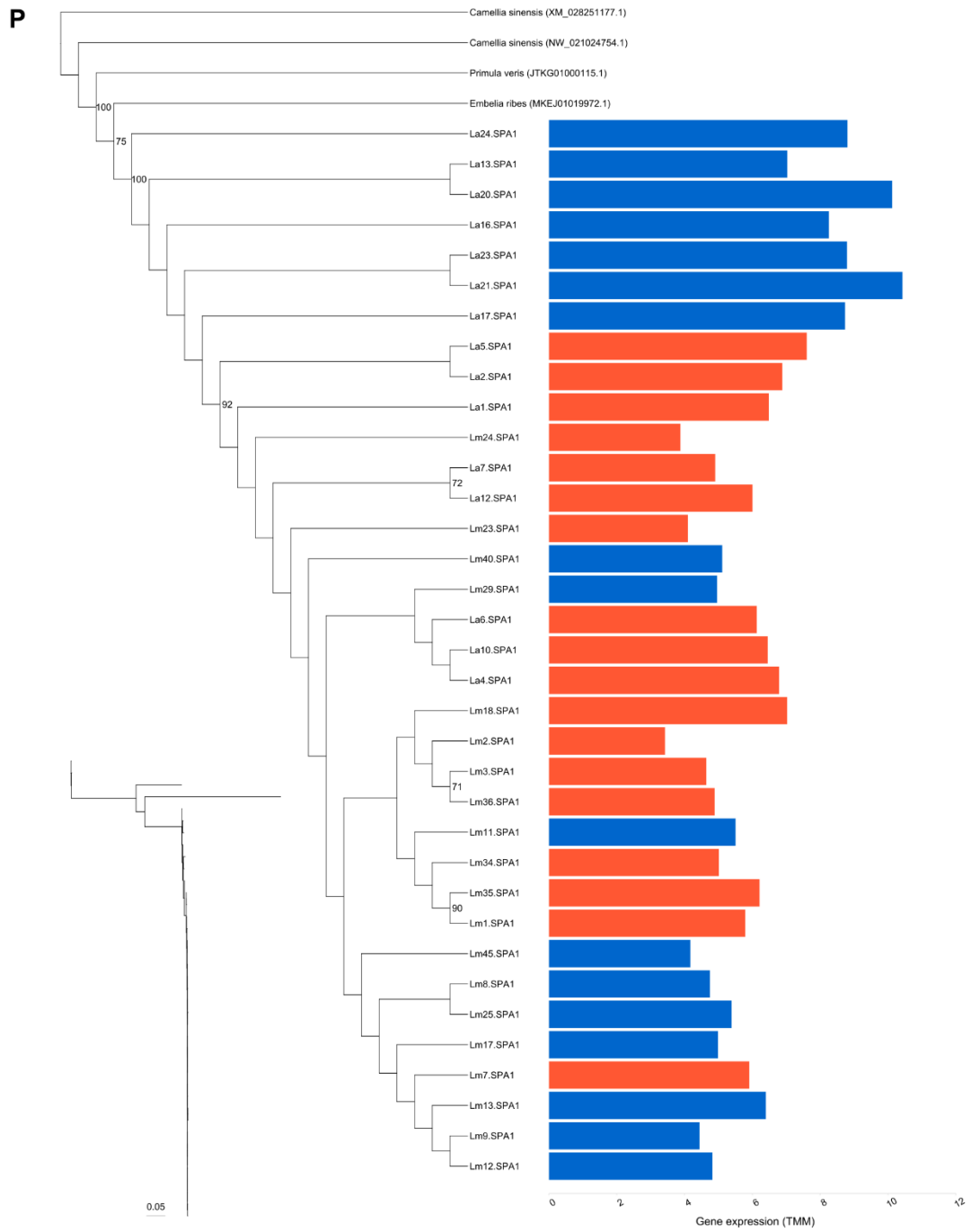
P
Camellia sinensis (XM_028251177.1)
Camellia sinensis (NW_021024754.1)
Primula veris (JTKG01000115.1)
Embelia ribes (MKEJ01019972.1)
La24.SPA1
La13.SPA1
La20.SPA1
La16.SPA1
La23.SPA1
La21.SPA1
La17.SPA1
La5.SPA1
La2.SPA1
La1.SPA1
Lm24.SPA1
La7.SPA1
La12.SPA1
Lm23.SPA1
Lm40.SPA1
Lm29.SPA1
La6.SPA1
La10.SPA1
La4.SPA1
Lm18.SPA1
Lm2.SPA1
Lm3.SPA1
Lm36.SPA1
Lm11.SPA1
Lm34.SPA1
Lm35.SPA1
Lm1.SPA1
Lm45.SPA1
Lm8.SPA1
Lm25.SPA1
Lm17.SPA1
Lm7.SPA1
Lm13.SPA1
Lm9.SPA1
Lm12.SPA1
100
75
100
92
72
71
90
0.05
0
2
4
6
8
10
12
Gene expression (TMM)

TTG1

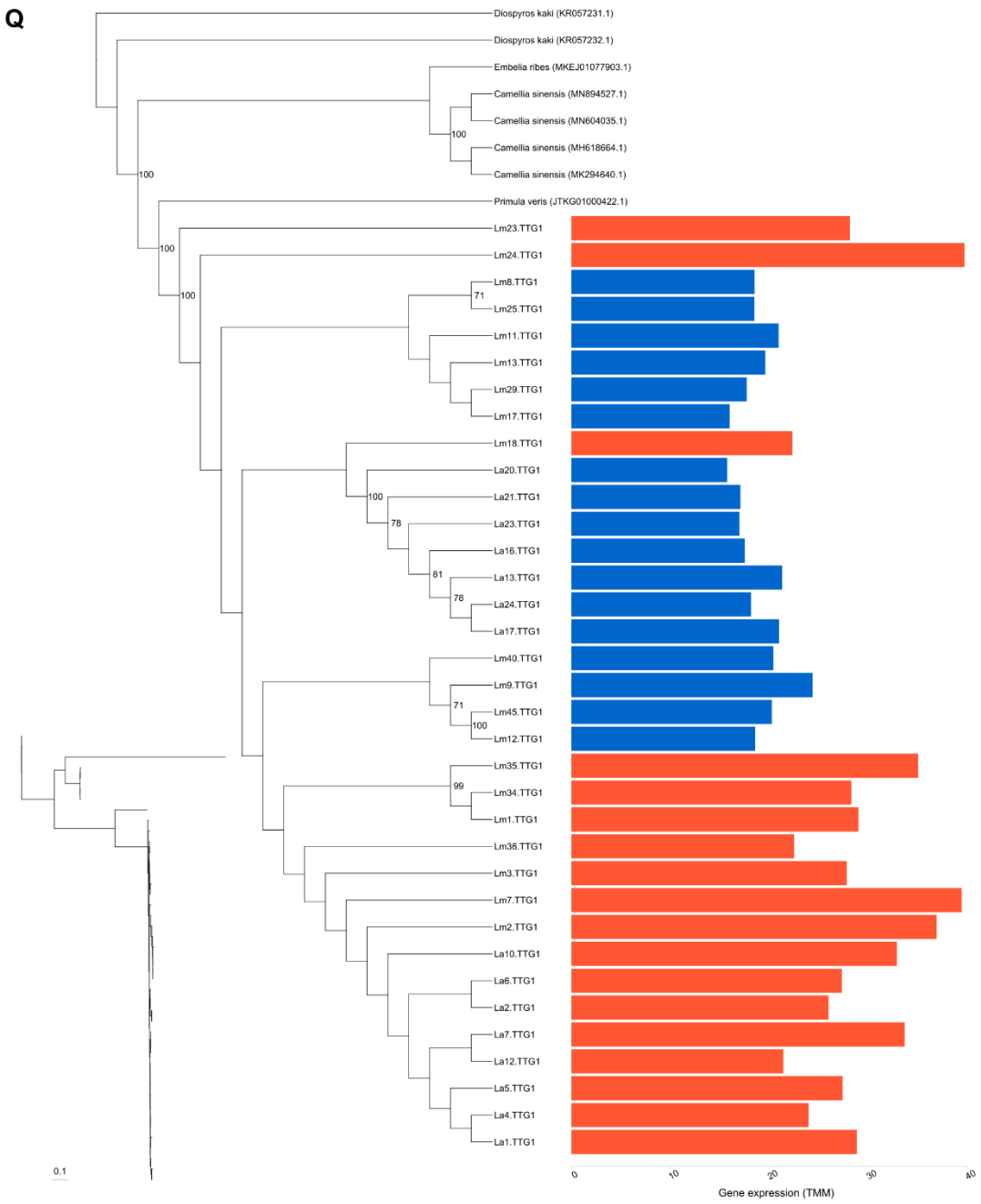

Appendix 1—figure 2. Maximum likelihood phylogenetic analysis of the coding sequence for eight structural (A-E) and 12 regulatory (F-Q) loci from blue and orange petals of *L. arvensis* and *L. monelli*. (A) *BZ1-2* and *-3*. (B) *Caffeoyl CoA-1,-2* and *-3*. (C) *CHS*. (D) *F3'5'H*. (E) *F3'H*. (F) *AN11a*. (G) *bHLH1*. (H) *bHLH2-2*. (I) *bHLH2-3*. (J) *bHLH12*. (K) *COP1*. (L) *MYB4-1*. (M) *MYB4-2*. (N) *MYB16-1*. (O) *MYB16-2*. (P) *SPA1*. (Q) *TTG1*. Outgroups were included when available from the genomes of closely

related species (*Camelia sinensis, Embelia ribes* and *Primula veris*). Bootstrap values above 70% are provided to the right of the nodes. Inset phylograms are provided for branch length comparisons with samples in same order as the larger cladogram and contain a scale bar in substitutions per site. The bar plots show the gene expression level (TMM values) of blue and orange flowers.

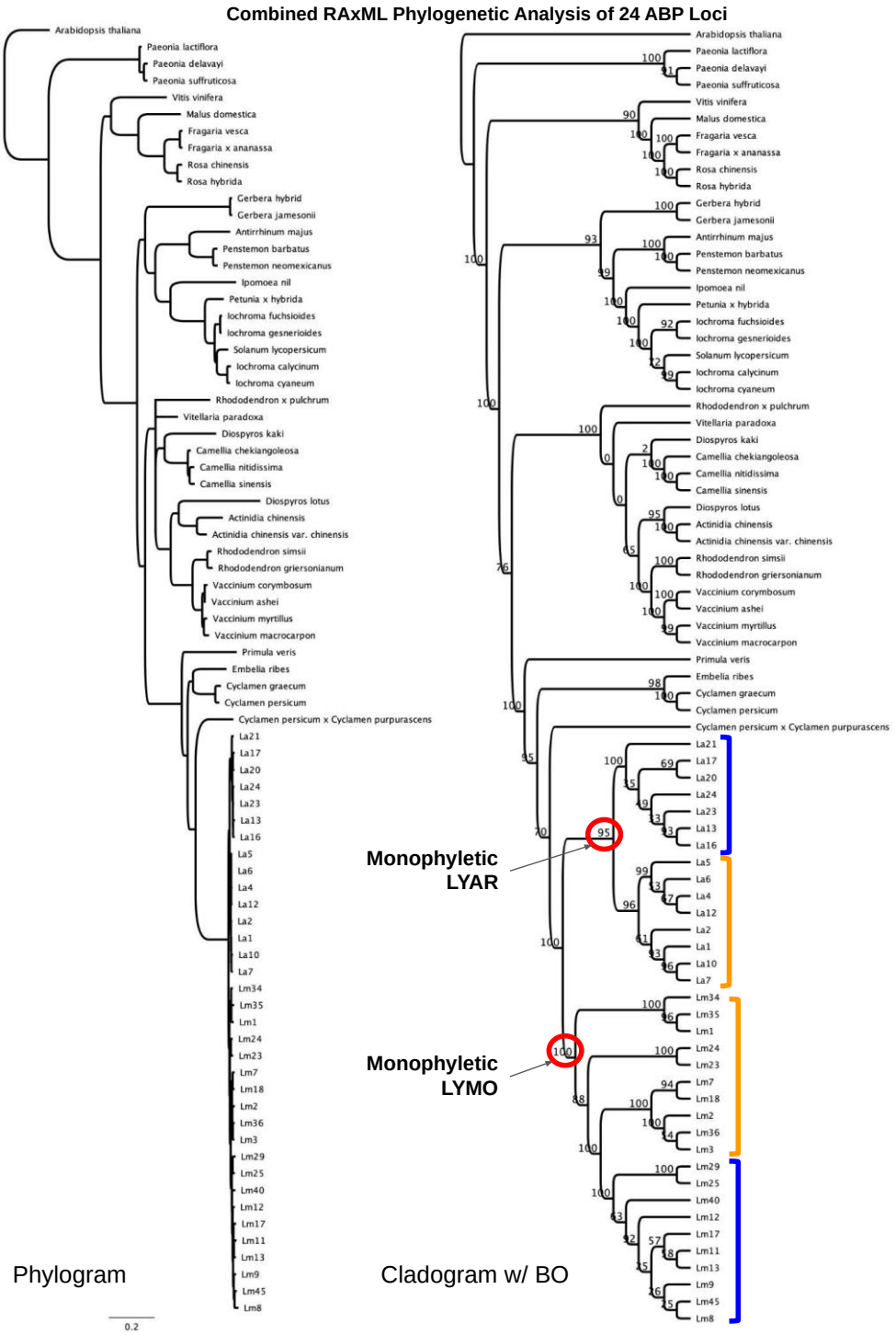

Appendix 1—figure 3. Combined maximum likelihood phylogenetic analysis of 24 ABP structural and regulatory loci. Phylogram on the left with branchlengths and cladogram on the right with bootstrap values indicated at the nodes. Cladogram annotated with petal color (blue and orange brackets). Lysimachia arvensis (LYAR and La samples) and L. monelli (LYMO and Lm samples) are strongly supported as monophyletic as are the color types within each species except for the paraphyly of LYMO orange.

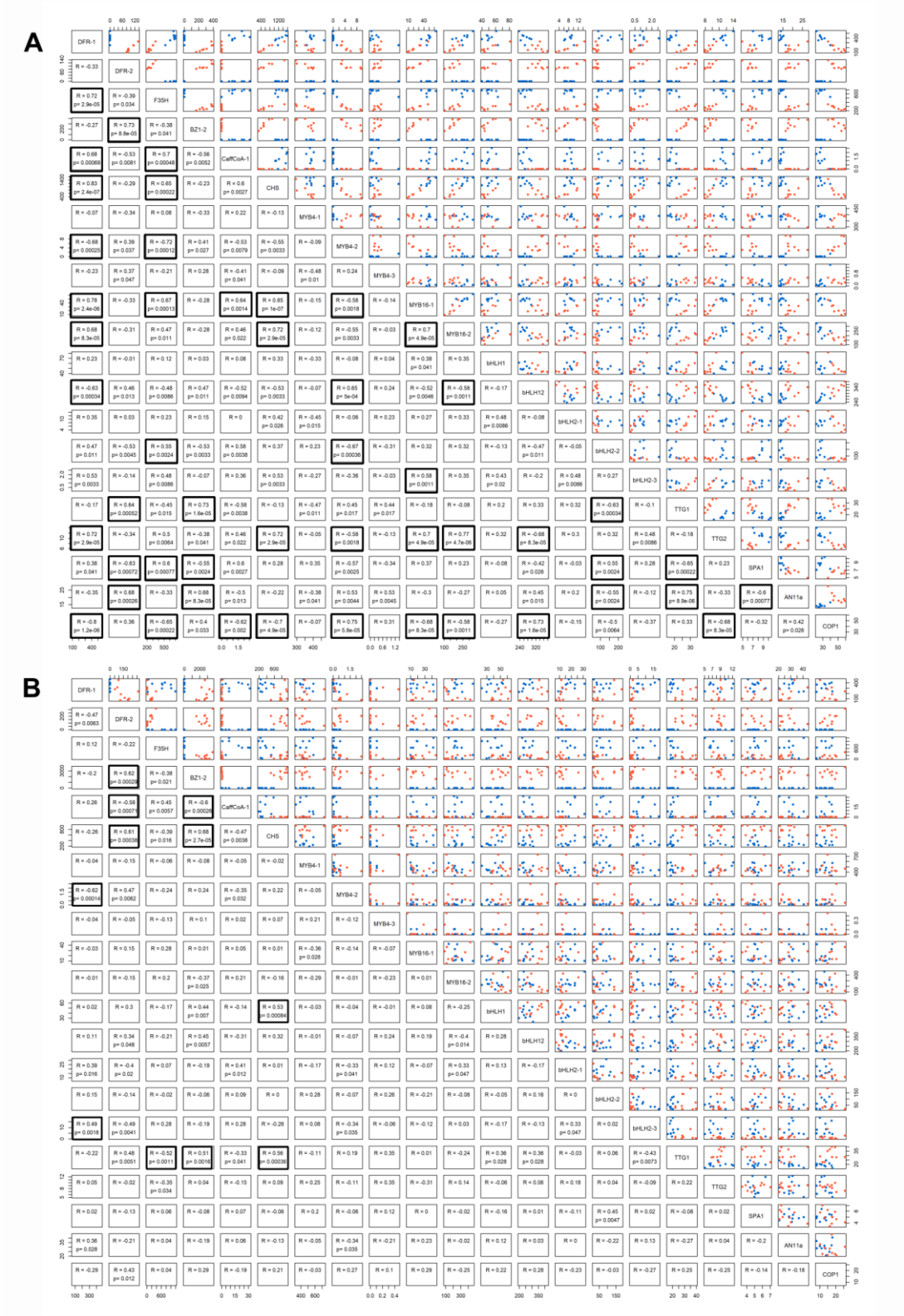

Appendix 1—figure 4. Kendall correlations of the expression level (TMM values) between the most relevant differential expressed structural genes (*DFR-1*, *DFR-2*, *F3'5'H*, *BZ1-2*, *CaffCoA-1*, *CHS*) and the regulatory genes (*MYB4-1*, *MYB4-2*, *MYB16-1*, *MYB16-2*, *bHLH1*, *bHLH12*, *bHLH2-1*, *bHLH2-2*, *bHLH2-3*, *TTG1*, *TTG2*, *SPA1*,

AN11a, *COP1*) present in blue and orange *L. arvensis* (A) and *L. monelli* (B). Correlation coefficients (R) and P values are listed below the diagonal and the raw data above the diagonal. Black boxes indicate those correlations that are significant following a Bonferroni correction.

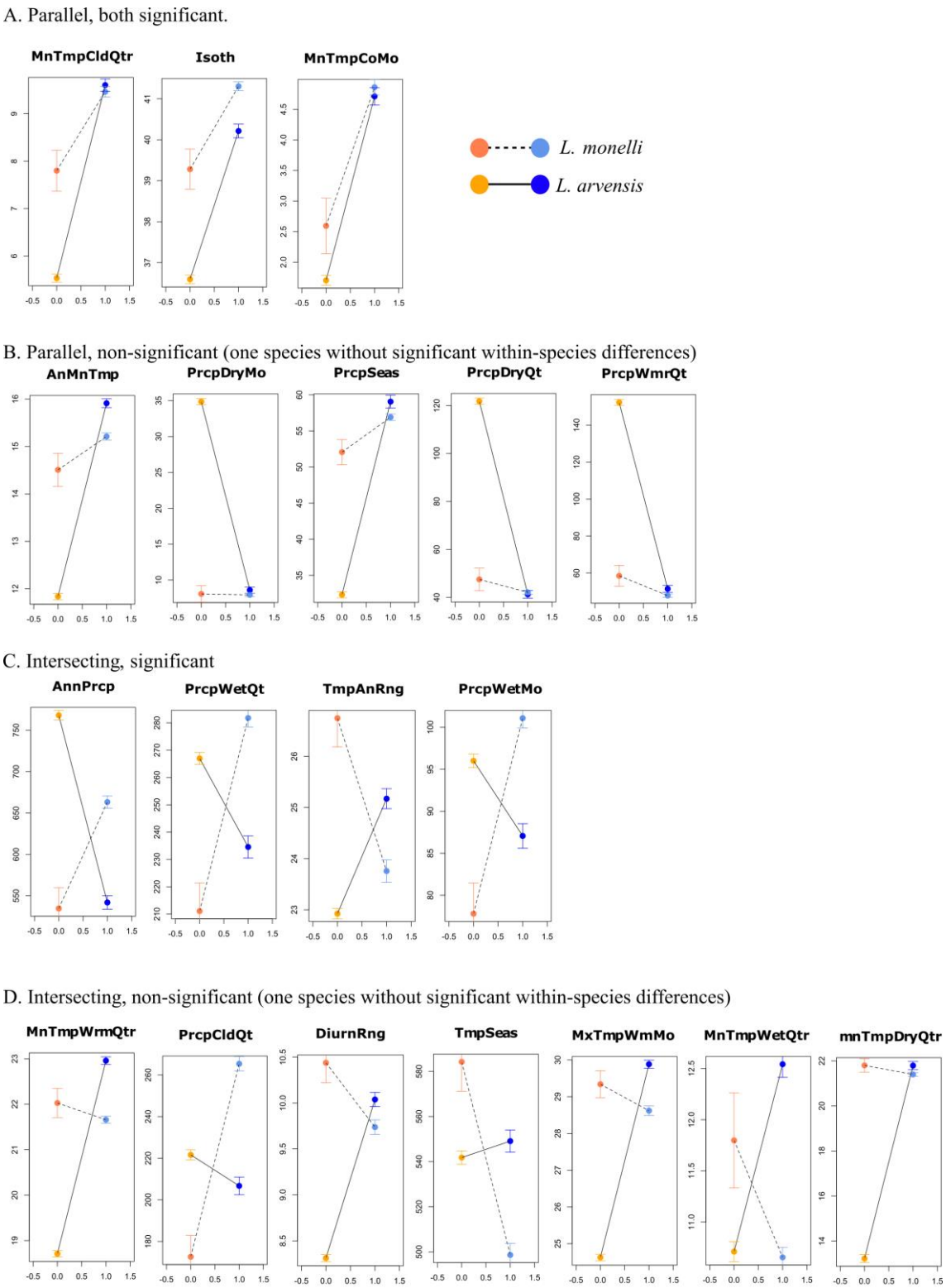

Appendix 1—figure 5. Climate niche modeling results for blue and orange morphs of *L. arvensis* and *L. monelli*. Grouped the 19 variables into 4 categories. (A) Parallel significant: slopes are similar (both + or both -), with orange/blue *L. monelli*

significantly different AND orange/blue *L. arvensis* significantly different. (B) Parallel non-significant: slopes are similar, one or both within-species comparison is non-significant. (C) Intersecting significant: slopes are different (one +, one -), within-species differences are significant. (D) Intersecting non-significant: Slopes are different, one within-species comparisons is non-significant.

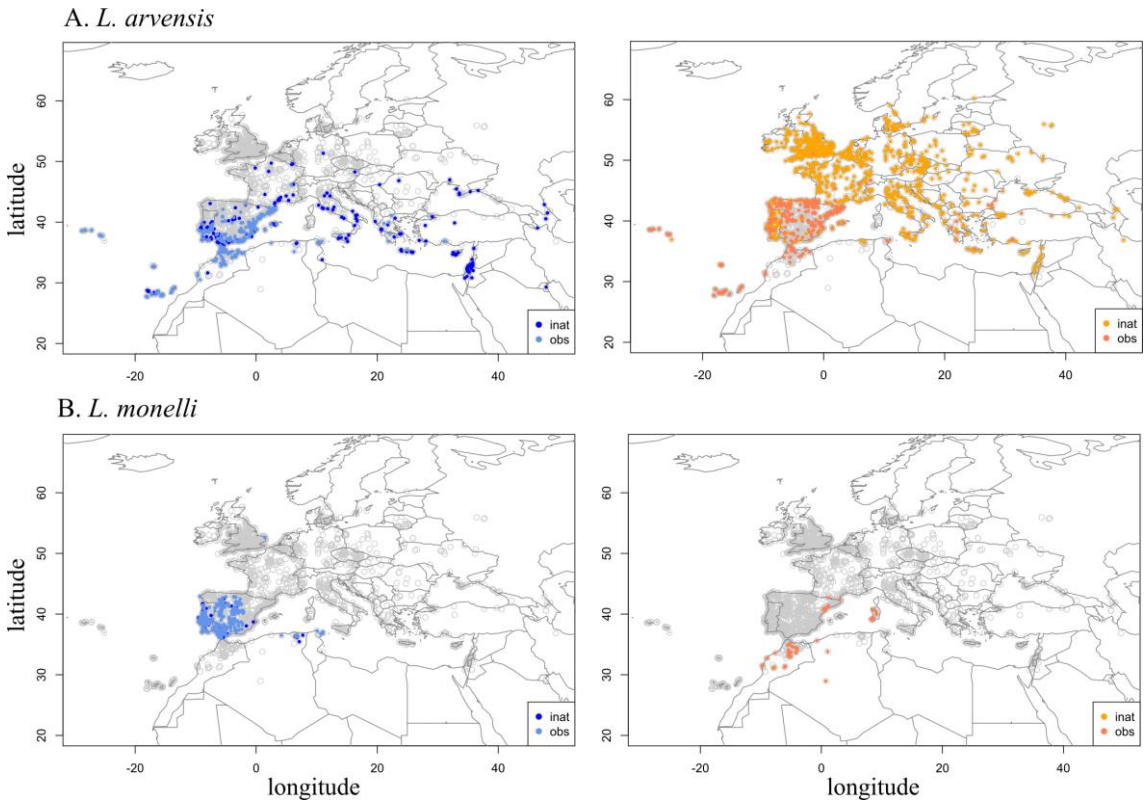

Appendix 1—figure 6. Occurrence data used in climate niche model from individually reviewed iNaturalist records and other sources (herbarium records, personal observations). For *L. arvensis*, there are 1941 orange occurrences and 641 blue (A). For *L. monelli*, there are 662 blues and 65 oranges.

Appendix 1—table 1. Putative flavonoid identifications of blue and orange petal extracts of *L. monelli* from the UHPLC–MS biochemical analysis (MS analysis was acquired in positive mode). Flavonoids <1% (trace) are not shown.

Petal color	Flavonoid class	Putative flavonoid identification	N samples**	t_R (min)	λ_{max} (nm)	Mass (m/z)	Relative content (%)***
Blue	Anthocyanin	Malvidin 3-rhamnoside	10/10	5.7	228, 278, 526	476.87	94.4
(**n** = 10 plants)	Anthocyanin	Delphinidin	10/10	2.1	229, 300, 521	variable	1.1
	Flavonol	Kaempferol 3-glucoside / Quercetin 3-rhamnoside / Isorhamnetin 3-pentoside / Luteolin 7-glucoside	5/10	7.7	226, 258, 291, 350	448.26	3.7
Orange	Anthocyanin	Pelargonidin 3-diglucoside	7/9	2.4	230, 277, 329, 426, 501	594.98	4.1
(**n** = 9 plants)	Anthocyanin	Pelargonidin 3-glucoside	9/9	3.1	231, 279, 429, 499	433.03	95.6

Identification was based on retention time (t_R), maximum absorbance wavelengths (λ_{max}) observed in the UV-Vis spectra of the compound that eluted at the t_R indicated, and molecular mass comparisons with standards and values of previously reported flavonoids for *Lysimachia* spp. (Sánchez-Cabrera et al., 2021 and the database http://metabolomics.jp).

*The fraction of samples containing each flavonoid.

**Relative content of each putative compound in each flower color, calculated from the area under the UV-Vis peaks.

Appendix 1—table 2. Flavonoid biosynthetic pathway genes with significant differential expression between blue- and orange-flowered *L. monelli*.

Gene abbreviation	Gene name	Blue expression (TMM)	Orange expression (TMM)	Log fold-change	Pathway
BZ1-2	*Anthocyanin 3-O-glucosyltransferase*	0.31	2651.84	-13.05	ABP
DFR-2	*Dihydroflavonol 4 reductase*	0.01	157.18	-12.53	ABP
CHS	*Chalcone synthase*	331.90	784.13	-1.24	ABP
Beta-glucosidase	*Beta-glucosidase*	0.09	4.13	-5.37	Non-ABP
Caffeoyl CoA-1	*Caffeoyl CoA-O-methyltransferase*	12.73	0.32	5.29	Non-ABP

Appendix 1—table 3. Summary of individual phylogenetic analyses of ABP structural and regulatory genes with high bootstrap support (>70%) indicating monophyletic clades in specific groups (genus, species, color). Genes showing orange monophyly (either for *L. arvensis*, *L. monelli* or both species) are highlighted in bold.

Genes	*Lysimachia*	La	La-O	La-B	Lm	Lm-O	Lm-B	O	B
Structural genes									
*BZ1-2***	100	98	-	-	-	-	-	100	-
BZ1-3	100	-	-	-	-	-	-	-	-
*Caff. CoA-1**	100	79	-	-	98	-	-	-	100
Caff. CoA-2	100	-	-	-	-	-	-	-	-
Caff. CoA-3	100	100	99	98	85	-	-	-	-
CHS	100	-	-	-	70	-	-	-	-
DFR-1	100	-	91	100	-	92	-	-	-
*DFR-2***	99	-	-	-	-	-	-	99	-
F3'5'H	100	-	98	86	93	-	-	-	-
F3'H	100	100	93	99	-	-	83	-	-
Regulatory genes									
AN11a	100	-	-	-	-	-	-	-	-
bHLH1	100	78	-	91	-	-	-	-	-
bHLH2-3	100	-	-	99	-	-	-	-	-
bHLH2-2	100	-	99	-	-	-	-	-	-
bHLH12	100	70	-	100	94	-	-	-	-
COP1	100	-	-	99	-	-	-	-	-
MYB4-1	99	-	-	-	-	-	-	-	-
MYB4-2	100	-	-	-	-	-	-	-	-

MYB16-1	100		-	87	-	-	-	-	-
MYB16-2	100	-	-	98	-	-	-	-	-
SPA1	100	-	-	-	-	-	-	-	-
TTG1	100	-	-	100	-	-	-	-	-

La (*L. arvensis*), Lm (*L. monelli*), O (orange), B (blue)

* Genes only present in blue petals

** Genes only present in orange petals

Appendix 1—table 4. Fixed non-synonymous SNPs in ABP loci that differentiate color morphs and those that differentiate species.

Gene	Position (aa)	Blue AA	Orange AA	BLOSUM62
Fixed Between Color Morphs				
DFR-1	279/287[a]	E	Q	+2
MYB4-2	361	M	I	+1
MYB4-2	376	P	S	-1
Fixed Between Species				
BZ1-3	435	K/A[b]	T	-1/0
CaffCoA-3	36	V	A	0
CaffCoA-3	200	F	Y	+3
CaffCoA-1 (only in blue)[c]	2	T	A	0
CaffCoA-1 (only in blue)	46	E	A	-1
CaffCoA-1 (only in blue)	215	T	A	0
CHS	363	R	L	-2
F3'H-1	19	S	Y	-2
F3'H-1	262	I	M	+1
F3'H-1	324	Q	H	0
F3'H-1	326	K	E	+1
F3'H-1	338	A	V	0
F3'H-1	341	R	L/P	-2/-2
F3'5'H	2	E	D	+2
MYB4-1	71	S	T	-1
MYB16-1	18	T	I	+1

[a] Two positions separated by a slash indicates the alignment position in *L. arvensis*/*L. monelli* (because of indels).

[b] Two amino acids separated by a slash indicates variable in one species (BLOSUM62 values are reported with a slash in the same order).

[c] "Only in blue" is reported when the locus was not detected in orange samples (still fixed between species, but only for blue).

Appendix 1—table 5. Results of hand-crosses between L. arvensis and L. monelli coming from different populations.

Mother species	Father species	Mother plant*	Father plant*	Mother color	Father color	Fruit production
L. monelli	*L. arvensis*	630/14_1	HIN_1.15	Blue	Blue	0
L. monelli	*L. arvensis*	630/14_2	HIN_1.15	Blue	Blue	0
L. monelli	*L. arvensis*	630/14_3	HIN_1.15	Blue	Blue	0
L. monelli	*L. arvensis*	630/14_4	HIN_2.21	Blue	Blue	0
L. monelli	*L. arvensis*	630/14_5	HIN_2.21	Blue	Blue	0
L. monelli	*L. arvensis*	630/14_1	COR_1.6	Blue	Orange	0
L. monelli	*L. arvensis*	630/14_2	COR_1.6	Blue	Orange	0
L. monelli	*L. arvensis*	630/14_3	COR_1.6	Blue	Orange	0
L. monelli	*L. arvensis*	630/14_4	COR_2.5	Blue	Orange	0
L. monelli	*L. arvensis*	630/14_5	COR_2.5	Blue	Orange	0
L. monelli	*L. arvensis*	151/14_1	HIN_1.15	Blue	Blue	0
L. monelli	*L. arvensis*	151/14_3	HIN_1.15	Blue	Blue	0
L. monelli	*L. arvensis*	151/14_4	HIN_2.21	Blue	Blue	0
L. monelli	*L. arvensis*	151/14_6	HIN_2.21	Blue	Blue	0
L. monelli	*L. arvensis*	151/14_7	HIN_8.7	Blue	Blue	0
L. monelli	*L. arvensis*	151/14_8	HIN_8.7	Blue	Blue	0
L. monelli	*L. arvensis*	151/14_1	COR_1.6	Blue	Orange	0
L. monelli	*L. arvensis*	151/14_3	COR_1.6	Blue	Orange	0
L. monelli	*L. arvensis*	151/14_4	COR_1.6	Blue	Orange	0
L. monelli	*L. arvensis*	151/14_6	COR_1.52	Blue	Orange	0
L. monelli	*L. arvensis*	151/14_7	COR_1.52	Blue	Orange	0
L. monelli	*L. arvensis*	151/14_8	COR_1.60	Blue	Orange	0
L. arvensis	*L. monelli*	HIN_1.15	630/14_1	Blue	Blue	0
L. arvensis	*L. monelli*	HIN_2.21	630/14_4	Blue	Blue	0
L. arvensis	*L. monelli*	HIN_2.21	630/14_5	Blue	Blue	0
L. arvensis	*L. monelli*	COR_1.6	630/14_1	Orange	Blue	0
L. arvensis	*L. monelli*	COR_2.5	630/14_5	Orange	Blue	0
L. arvensis	*L. monelli*	HIN_1.15	151/14_1	Blue	Blue	0
L. arvensis	*L. monelli*	HIN_1.15	151/14_3	Blue	Blue	0

L. arvensis	*L. monelli*	HIN_2.21	151/14_4	Blue	Blue	0
L. arvensis	*L. monelli*	HIN_8.7	151/14_8	Blue	Blue	0
L. arvensis	*L. monelli*	COR_1.6	151/14_1	Orange	Blue	0
L. arvensis	*L. monelli*	COR_1.6	151/14_3	Orange	Blue	0
L. arvensis	*L. monelli*	COR_1.52	151/14_6	Orange	Blue	0
L. arvensis	*L. monelli*	COR_1.60	151/14_8	Orange	Blue	0
L. monelli	*L. arvensis*	485/14_1	HIN_1.15	Orange	Blue	0
L. monelli	*L. arvensis*	485/14_1	HIN_1.15	Orange	Blue	0
L. monelli	*L. arvensis*	485/14_2	HIN_2.21	Orange	Blue	0
L. monelli	*L. arvensis*	485/14_2	HIN_2.21	Orange	Blue	0
L. monelli	*L. arvensis*	485/14_3	HIN_8.7	Orange	Blue	0
L. monelli	*L. arvensis*	485/14_3	HIN_8.7	Orange	Blue	0
L. monelli	*L. arvensis*	485/14_1	COR_1.6	Orange	Orange	0
L. monelli	*L. arvensis*	485/14_1	COR_1.6	Orange	Orange	0
L. monelli	*L. arvensis*	485/14_2	COR_1.52	Orange	Orange	0
L. monelli	*L. arvensis*	485/14_2	COR_1.52	Orange	Orange	0
L. monelli	*L. arvensis*	485/14_3	COR_1.60	Orange	Orange	0
L. monelli	*L. arvensis*	485/14_3	COR_1.60	Orange	Orange	0
L. arvensis	*L. monelli*	HIN_1.15	485/14_1	Blue	Orange	0
L. arvensis	*L. monelli*	HIN_2.21	485/14_2	Blue	Orange	0
L. arvensis	*L. monelli*	HIN_8.7	485/14_3	Blue	Orange	0
L. arvensis	*L. monelli*	COR_1.6	485/14_1	Orange	Orange	0
L. arvensis	*L. monelli*	COR_1.52	485/14_2	Orange	Orange	0
L. arvensis	*L. monelli*	COR_1.60	485/14_3	Orange	Orange	0

*Population information:

- HIN: L. arvensis. Spain, Huelva, Hinojos (37º17'42.6"N, 6º58'05"W)
- COR: L. arvensis. France, Corsica, Solenazara (41°51'19.6"N, 9°21'43.7"E)
- 630/14: L. monelli. Spain. Cádiz. Barbate. Breña de Barbate (36°10'39.3"N, 5°58'56.1"W)
- 485/14: L. monelli. Spain. Tarragona. Mont-Roig (41º5'18"N, 0º56'5"E)
- 151/14: L. monelli. Portugal. Natural Reserve das Lagoa de St André (38º0'55.2"N, 8º49'11.1"W)

Appendix 1—**table 6**. Climatic differences among morphs. Comparisons indicate significance of differences among morphs (e.g. between the two orange morphs or between the two color morphs within *L. arvensis*) and were Bonferroni adjusted for 76 comparisons (nineteen variables x four morph comparisons).

	Variable means (SE)				Morph Comparisons (Kruskal Wallis p values)			
	arvensis orange	arvensis blue	monelli orange	monelli blue	arvensis difference	orange difference	blue difference	monelli difference
AnMnTmp	11.839 (0.067)	15.912 (0.093)	14.508 (0.35)	15.21 (0.076)	< 0.001	< 0.001	< 0.001	1.0
MnTmpWrmQtr	18.71 (0.07)	22.96 (0.083)	22.027 (0.32)	21.659 (0.077)	< 0.001	< 0.001	< 0.001	1.0
MnTmpCldQtr	5.534 (0.084)	9.604 (0.129)	7.8 (0.432)	9.464 (0.11)	< 0.001	< 0.001	1.0	0.04
AnnPrcp	768.135 (5.65)	541.901 (8.085)	534.675 (25.145)	663.231 (7.37)	< 0.001	< 0.001	< 0.001	0.002
PrcpWetMo	96.007 (0.794)	87.062 (1.458)	77.805 (3.642)	101.085 (1.169)	< 0.001	0.003	< 0.001	< 0.001
PrcpDryMo	34.857 (0.427)	8.609 (0.441)	8.078 (1.151)	7.946 (0.243)	< 0.001	< 0.001	1.0	1.0
PrcpSeas	32.321 (0.425)	59.064 (0.891)	52.067 (1.748)	56.902 (0.445)	< 0.001	< 0.001	1.0	1.0
PrcpWetQt	266.99 (2.216)	234.572 (4.038)	211.078 (10.287)	281.789 (3.318)	< 0.001	< 0.001	< 0.001	< 0.001
PrcpDryQt	121.847 (1.295)	41.244 (1.606)	47.494 (4.703)	42.091 (0.853)	< 0.001	< 0.001	1.0	1.0
PrcpWmrQt	152.319 (1.603)	51.462 (1.897)	58.494 (5.645)	47.816 (0.897)	< 0.001	< 0.001	1.0	1.0
PrcpCldQt	221.595 (2.408)	206.694 (4.206)	172.61 (10.381)	265.361 (3.44)	0.582	0.022	< 0.001	< 0.001
DiurnRng	8.312 (0.038)	10.038 (0.077)	10.438 (0.217)	9.737 (0.08)	< 0.001	< 0.001	1.0	0.698
Isoth	36.593 (0.107)	40.213 (0.167)	39.281 (0.491)	41.305 (0.108)	< 0.001	< 0.001	0.002	0.05
TmpSeas	541.797 (2.946)	549.092 (4.9)	584.242 (13.062)	498.631 (5.108)	1.0	1.0	< 0.001	< 0.001
MxTmpWmMo	24.626 (0.087)	29.884 (0.11)	29.34 (0.366)	28.619 (0.13)	< 0.001	< 0.001	< 0.001	1.0
MnTmpCoMo	1.703 (0.081)	4.712 (0.142)	2.594 (0.454)	4.862 (0.126)	< 0.001	1.0	1.0	< 0.001
TmpAnRng	22.923 (0.104)	25.172 (0.195)	26.747 (0.56)	23.757 (0.219)	< 0.001	< 0.001	< 0.001	< 0.001

MnTmpWetQtr	10.711 (0.098)	12.542 (0.128)	11.798 (0.465)	10.655 (0.097)	< 0.001	1.0	< 0.001	1.0
mnTmpDryQtr	13.224 (0.178)	21.795 (0.179)	21.802 (0.297)	21.399 (0.08)	< 0.001	< 0.001	1.0	1.0

Appendix 1—table 7. Logistic regression models for each species on a subset on non-correlated climate variables. The best models using AIC for *L. arvensis* (Arv) and *L. monelli* (Mon) are presented. "Good models" have lower, but close AIC values and reinforce the importance of the variables included in the best model.

***L. arvensis* Best Model**

Coefficients	Estimate	Std. Error	z value	p
Intercept	14.5510859	0.8911108	16.33	< 0.0001
PrcpSeas	-0.0453151	0.0028234	-16.05	< 0.0001
Isoth	-0.1980946	0.0168407	-11.76	< 0.0001
TmpSeas	-0.0070202	0.0005796	-12.11	< 0.0001

***L. arvensis* Good Models**

Intercept	Isoth	MeanTemp WarmQtr	PrcpSeas	PrcWarm Mon	TmpSeas	df	Delta AIC
47.92	20.240		-37.950	2.044	-46.670	5	1.20
58.550	18.270	1.649	-39.18		-57.010	5	1.96
45.220	19.610	5.531	-37.94	2.695	-44.090	6	2.80

***L. monelli* Best Model**

Coefficients	Estimate	Std. Error	z value	p
Intercept	-1.568856	0.635342	-2.469	0.0135
PrcpWetMo	-0.035533	0.005195	-6.840	< 0.0001
MnTmpWetQtr	0.229809	0.049652	4.628	< 0.0001

***L. monelli* Good Models**

Intercept	Isoth	MeanTemp WarmQtr	PrcpSeas	PrcWarm Mon	TmpSeas	df	Delta AIC
22.280	-81.070	215.70	20.42	-24.93	-20.80	6	1.68
46.480	-89.320	210.80		-24.22	-44.92	5	5.67
-0.02067	-70.320	210.30		-17.75		4	5.82

Appendix 1—table 8. Significance values from randomization tests indicating whether orange or blue populations are more different from one another climatically than expected by chance.

	Orange divergent	Blue divergent	Conclusion
AnMnTmp	< 0.001	0.999	Orange more divergent
MnTmpWrmQtr	< 0.001	0.999	Orange more divergent
MnTmpCldQtr	< 0.001	0.999	Orange more divergent
AnnPrcp	< 0.001	0.999	Orange more divergent
PrcpWetMo	0.205	0.794	Not Significant
PrcpDryMo	< 0.001	0.999	Orange more divergent
PrcpSeas	< 0.001	0.999	Orange more divergent
PrcpWetQt	0.039	0.96	Orange more divergent
PrcpDryQt	< 0.001	0.999	Orange more divergent
PrcpWmrQt	< 0.001	0.999	Orange more divergent
PrcpCldQt	0.796	0.203	Not significant
DiurnRng	< 0.001	0.999	Orange more divergent
Isoth	< 0.001	0.999	Orange more divergent
TmpSeas	0.702	0.297	Not significant
MxTmpWmMo	< 0.001	0.999	Orange more divergent
MnTmpCoMo	0.410	0.958	Not significant
TmpAnRng	< 0.001	0.999	Orange more divergent
MnTmpWetQtr	0.999	< 0.001	Blue more divergent
MnTmpDryQtr	< 0.001	0.999	Orange more divergent

Appendix 1—table 9. Plant population locations and herbarium accession numbers for *Lysimachia monelli* samples used for RNA-seq and UHPLC-MS (flavonoid profiling) (marked with a X). Voucher specimens were deposited in the University of Seville Herbarium (SEV).

Population	Color	Country	Location	Lat.	Long.	RNA-Seq	UHPLC-MS	**Accession #**
1/17-MS	Blue	Spain	Huelva. Almonte	37.055472	-6.541722	X	X	SEV285033
2/17-MS	Blue	Spain	Huelva. Pinares de Hinojos	37.217917	-6.417889	X	X	SEV287947
3/17-MS	Blue	Spain	Sevilla. Bormujos	37.371861	-6.082139	X	X	SEV287606
4/17-MS	Blue	Spain	Sevilla. Bellavista	37.330694	-5.964528		X	SEV287605
6/17-MS	Blue	Spain	Sevilla. Dos Hermanas	37.275042	-5.932889	X	X	SEV286835
7/17-MS	Blue	Spain	Cádiz. Carretera entre Borneo y Espera	36.836028	-5.752167		X	SEV286849
10/17-MS	Blue	Spain	Sevilla. Entre los Molares y Utrera. Km 5	37.162364	-5.760236	X	X	NA
LM_8	Blue	Spain	Cádiz. Barbate. Breña de barbate	36.177583	-5.982250	X	X	SEV286494
LM_24	Blue	Portugal	Carrapateira	37.193333	-8.905278	X	X	SEV286463
LM_28	Blue	Portugal	Sainto André	38.015333	-8.819750		X	SEV284791
ES_19	Orange	Spain	Tarragona. Urb. Sant Jordi D'Alfama	40.924883	0.813133	X		SEV285130
SAR_2	Orange	Italy	Sardinia. Isola de Sant Pietro, Cala Fico	39.154967	8.228783	X	X	SEV287100

SAR_3	Orange	Italy	Sardinia. Isola de Sant Pietro, Cabo Sandalo, Faro	39.144100	8.224050	X	X	SEV287102
SAR_6	Orange	Italy	Sardinia. Sa Duchesa	39.372417	8.597500	X	X	SEV287085
MAR_2	Orange	Morocco	Carretera de El Hajeb a Azrou	33.527778	-5.306944		X	SEV289309
MAR_4	Orange	Morocco	Rif. Chefchaouene	35.183767	-5.224550		X	SEV289310
MAR_8	Orange	Morocco	Medio Atlas. Kenifra. Entre Boufekran y Kenifra	33.618217	-5.430767	X	X	SEV289311
MAR_10	Orange	Morocco	Rif. Ouezzane	34.880000	-5.530000		X	SEV289312
MAR_12	Orange	Morocco	Medio Atlas. Kenifra	33.027933	-5.324650		X	SEV289314
MAR_30	Orange	Morocco	Zerhoun	34.069083	-5.455567		X	SEV289315

Appendix 1—table 10. Summary of sequencing and assembly results for the 20 *L. monelli* petal samples.

Sample	Population	Flower color	Number of reads	Number of filtered reads	Filtered reads aligned to the assembly (%)	Number of transcripts	Number of trinity genes*
Lymo_1	ES_19	orange	19,356,011	18,421,349	92.48	47,377	26,986
Lymo_2	SAR_3	orange	17,662,750	16,866,036	93.30	45,323	27,137

Lymo_3	SAR_2	orange	18,038,810	17,237,553	93.16	48,194	29,126
Lymo_7	SAR_6	orange	17,084,149	16,312,231	92.11	49,194	29,265
Lymo_18	SAR_6	orange	17,166,042	16,255,988	90.86	48,459	28,927
Lymo_23	MAR_8	orange	16,537,229	15,503,176	92.47	48,701	28,213
Lymo_24	MAR_8	orange	16,709,072	15,886,953	92.23	49,265	28,074
Lymo_34	ES_19	orange	17,230,125	16,466,487	92.21	49,477	28,830
Lymo_35	ES_19	orange	23,467,043	22,697,727	92.73	46,959	27,097
Lymo_36	SAR_2	orange	16,981,334	15,773,601	92.57	52,169	31,542
Lymo_40	2/17-MS	blue	18,359,772	17,602,178	93.03	46,380	26,228
Lymo_45	LM_8	blue	17,828,507	16,984,718	92.32	48,951	28,143
Lymo_8	LM_24	blue	16,850,071	16,124,259	91.26	45,973	26,624
Lymo_9	1/17-MS	blue	18,050,225	17,338,160	92.84	45,891	26,354
Lymo_11	6/17-MS	blue	19,073,958	18,182,529	92.42	47,224	26,815
Lymo_12	LM_8	blue	18,350,299	17,810,293	93.54	44,695	25,856

Lymo_13	10/17-MS	blue	17,255,892	16,498,600	92.63	46,720	26,591
Lymo_17	3/17-MS	blue	17,405,546	16,803,173	93.02	47,313	27,096
Lymo_25	3/17-MS	blue	16,982,762	15,953,718	92.29	48,271	27,650
Lymo_29	6/17-MS	blue	16,331,233	15,578,920	93.01	45,869	25,935

* Trinity genes were limited to those having TMM > 1.